



Machinability Investigation and Sustainability Assessment of Dry Cutting AISI1045 Steel Using Tools Configured with Shark-Skin-Inspired Structures and WS₂/C Coatings

Xuemu Li¹ · Jianxin Deng¹ · Yang Lu¹ · Ran Duan² · Dongliang Ge¹

Received: 27 June 2020 / Revised: 24 January 2021 / Accepted: 18 February 2021 / Published online: 15 March 2021
© Korean Society for Precision Engineering 2021

Abstract

This paper primarily determined the suitable technique for the preparation of WS₂/C coating by the analytical hierarchy process (AHP) with a keen focus on the criteria of coating property, deposition process, resource and equipment. Further, some cutting performances of six cutting tools with different treatments, including cutting forces, cutting temperatures, wear mechanisms, tool life, etc. were investigated in dry cutting AISI1045 steel. The optimal lubricating condition for dry cutting process was obtained when using the cutting tools configured with the combination of WS₂/C coating and shark-skin-inspired structures. Finally, the sustainability assessment was carried out by the calculation of the product sustainability index (PSI). The highest PSI of 78.6% was obtained in case of the dry cutting experiment using WMT-2-N tools, which provided a suggested favorable alternative considering both product and manufacturing process. Thus, dry cutting AISI1045 steel using WMT-2-N tools seems to be an environmentally-friendly machining process and would be helpful to enhance sustainability.

Keywords WS₂/C coatings · Shark-skin-inspired structures · Self-lubricating tool · Dry cutting performance · Sustainability assessment

Abbreviations

γ_0	Rake angle (deg)
α_0	Clearance angle (deg)
κ_r	Cutting edge angle (deg)
λ_s	Edge inclination angle (deg)
f	Feed rate (mm/r)
a_p	Depth of cutting (mm)
ν	Cutting speed (m/min)
F_f	Feed force (N)
F_p	Radial thrust force (N)
F_c	Tangential force (N)
μ	Tool-chip friction coefficient
ϕ	Shear angle (deg)
ξ	Chip thickness ratio
a_{ch}	Deformed chip thickness (mm)

a_{cp}	Undeformed chip thickness (mm)
N	Spindle speed (rpm)

1 Introduction

Sustainable manufacturing has been one recognized trend for today's manufacturing practice due to some emerging demands: protecting environment and improving occupational safety/health, reducing the consumption of the non-renewable resources and overall manufacturing cost, etc. [1, 2]. Sustainable manufacturing was defined by the U.S. Department of Commerce as [3] "the creation of manufactured products that use processes that minimize negative environmental impacts, conserve energy and natural resources, are safe for employees, communities, and consumers and are economically sound." Metal cutting, as one of the most common and major process manner in mechanical manufacture, has been expected to increase its importance as the product cycles become shorter and the processing systems become more flexible. During the metal cutting, cutting fluid is widely used for lubrication and cooling. It is estimated that ~640 million gallons of cutting fluid is annually consumed in the world [4], and most

✉ Jianxin Deng
jxdeng@sdu.edu.cn

¹ Key Laboratory of High Efficiency and Clean Mechanical Manufacture of MOE, School of Mechanical Engineering, Shandong University, Jinan 250061, China

² School of Mechanical and Electronic Engineering, Shandong Jianzhu University, Jinan 250061, China

of them are extracted from the unsustainable crude oil [5]. Storing, cleaning and disposal of the cutting fluid are tedious and time-consuming. The cutting fluids account for 7–17 % in the total cost of the manufacturing process, while it is 2–4 % for the cutting tools [6, 7]. Moreover, rampant uses or improper disposal will bring harm to the environment and operator health. National Institute of Occupational Safety and Health has reported that the cutting fluid was harming over 1 million workers, and they were the main potential cause of skin and chest bronchitis diseases of the operators [8]. Therefore, it is urgent practice to substantially reduce the use of cutting fluids from the environment, personnel safety/health, cost, resources consumption and waste management point of view. Dry cutting, following the conception of sustainable manufacturing, could be helpful to build environment-friendly processing mode, reduce cost and promote operational satisfaction of the workers. Although dry cutting is an eco-friendly technique, there are still some drawbacks to be solved. Due to the lack of cutting fluids, the stress and temperature would be elevated between tool face and chip or workpiece, resulting in severe tool wear [9–11]. The damaged tools would not only reduce the removal rate of the workpieces, but deteriorate surface integrity of the machined products as well. Moreover, the shortened tool life increases the manufacturing costs. To develop high-performance dry cutting tools have been needed for sustainability.

Surface coating technology, as a kind of surface engineering technique, can be applied to meet the multi-functional requirements in the technical fields of biochemistry, medicine and manufacture [12–14]. In the case of metal cutting specifically, by designing and using a variety of composite or nanostructured lubricating coatings, reduced friction and wear loss would be obtained, resulting in fuel economy, improved tool durability and sustainability for metal cutting. Transition metal (TM) sulfides, especially MoS_2 and WS_2 , can be used as lubricating coatings due to their well-defined layered structures [15–17]. When the temperature reaches above 400 °C, MoS_2 would be easily oxidized to MoO_3 , which could decrease the lubricating ability of the lubricating coatings. WS_2 exhibits lower average friction coefficients and could withstand higher temperature (650 °C in the air medium) [18]. WO_3 is preferred to MoO_3 , as it can provide a lower friction coefficient and be more protective than MoO_3 [15]. Increased lubricity of the transition metal sulfides has been obtained by incorporating with metals (such as Cr [19] or Zr [20]) or nonmetals (such as N [21] or carbon [22]). Not only these elements could improve the mechanical properties of the coatings, but they also can enhance their anti-oxygenic ability by preferential oxidation. Nowadays various fabrication techniques have been applied to coating deposition for cutting tools. The widely applied method is physical vapour deposition (PVD), such as magnetron deposition and cathode-arc deposition.

Electrohydrodynamic atomization (EHDA) deposition, first reported by Zeleny [23], is a dynamic atomization process of electric fluid where micro-fluid is pulled and broken into tiny droplets when the liquid surface tension is overcome by the electric fluid force. Because of the advantages of high deposition efficiency, strong controllability and easy availability of slurry, EHDA has shown great potential for coating fabrication. In our previous studies [24, 25], WS_2 coatings with the thickness above 20 μm were fabricated by the EHDA technique and showed good lubricating properties.

Surface texturing or structuring is another method to improve the sustainability of dry cutting [26, 27]. Different types of microstructures engraved on the surfaces of the cutting tools have shown the effect in lowering sliding friction, reducing tool-chip contact length, promoting heat dissipation and relieving adhesive wear. Kawasegi et al. [28] fabricated three types of patterns (parallel, perpendicular and cross patterns) on the rake face of the cutting tools. It was found that the textures perpendicular to the chip flow was beneficial to reduce cutting force. Deng et al. [29] produced three rake-face textured tools with different micro structures and found that the elliptical grooves promoted better dry cutting performance than the parallel or linear grooves. Sugihara et al. [30] prepared some dimples on the rake face of the cutting tools. A series of experiments about dry cutting aluminum alloys revealed that the textured tools exhibited superior cutting properties, especially suppressing aluminum adhesion, compared with those with groove textures. Nature has provided us with multiple examples of textured surfaces which are optimized for tribology by the combination of texture type and distribution, such as the surfaces of sharkskin, ball python skin and sandhoppers' cuticle surface [31–33]. Fatima et al. [32] fabricated structures resembling the scales of snake skin on the flank face of the cutting tools by laser machining. Some benefits such as reduced cutting forces, tool wear, temperature, iron adhesion were obtained. However, the patterns were isolated from each other, which would be unfavorable for wear debris flow and collection. Lu et al. [34] fabricated a biomimetic engineering surface comprising both the shark-skin, the shark body denticle, and rib morphology. The pin-on-disk rubbing experiments showed that these textures could help reduce water resistance and the friction contact area as well as accommodate lubricant oil. In our previous studies [24, 35], the Al_2O_3 and ZrO_2 surfaces with shark-skin-inspired structures were fabricated by laser machining. The effect of the shark-skin-inspired structures on improving friction and wear property of the surfaces was verified by dry sliding experiments. These studies throws enlightenment for improving dry cutting properties by creating biomimetic structures on the surfaces of cutting tools. However, very limited research works have been reported concerning dry cutting with cutting tools configured with shark-skin-inspired structures and WS_2/C coatings, which plays a very important role for improvement of machinability. It remains

to be explored to ensure the metal cutting process towards a sustainable manufacturing mode. Thus, this paper would not only focus on the machining performance, but also considers the sustainability aspects.

In this paper, the dry cutting tools with the synergy of WS_2/C lubricant coatings and shark-skin-inspired structures were developed. Firstly, the shark-skin-inspired structures were fabricated on the tool face by laser engraving. Then, the method of multi-criteria analysis, called analytic hierarchy process (AHP) [36], was used to compare the PVD technique (magnetron deposition and cathode-arc deposition) with EHDA technique and the optimal one was chosen. The dry cutting properties, including cutting forces, cutting temperatures, friction coefficient and shear angle were investigated. The product sustainability index (PSI) was calculated for the sustainability evaluation of dry cutting AISI1045 steel using different tools. This study can provide one sustainable dry-cutting method by using tools configured with biomimetic surfaces and lubricating coatings. If possible, this cutting tool with the synergistic effect of shark-skin-inspired structures and WS_2/C coatings could be applied industrially in the future.

2 Experimental details

2.1 Fabrication of cutting tools with shark-skin-inspired structures

The WC/Co cemented carbide cutting tools were used for dry-cutting AISI1045 steel in this paper, and their properties were shown in Table 1. As shown in Fig. 1a, firstly, depending on the structures of the shark skin [34], the idealized shark-skin-inspired structure with micro-grooves nested within rhombuses cells was designed and prepared on the rake face by laser engraving (wavelength = 1064 nm, average power = 4 W, repetition rate = 20 kHz and scanning speed = 100 mm/s). The sharkskin-like biomimetic textures were selected because: (1) the rhombus structures imitating the bionic placoid structure could improve the drag reduction characteristic, (2) the grooves located in the rhombus structures imitating the rib structures could reduce friction area and shear stress, (3) the height different between grooves and rhombus structures would make the change gap in the contact area and be favorable for debris flow, and (4) the grooves acted as wear debris collector could minimize abrasive wear. After micro-texturing, the cutting tools were polished and cleaned in order to get rid of the slags and to reduce the surface roughness. Then the nano-grooves simulating nano-textures of the shark skin were

fabricated and spread across the micro-textures by a femto-second laser system (Legend Elite-USP, Coherent Inc., USA). The scanning speed, pulse energy and scanning interval of the femtosecond laser was 100 $\mu\text{m/s}$, 2.5 μJ and 5 μm , respectively, and its scanning direction was perpendicular to the main cutting edge. In order to analyze the influence of groove direction on cutting performance, four kinds of textured tools are prepared and shown in Table 2.

2.2 Deposition of the WS_2/C coatings

The optimum deposition technique for lubricating coatings was selected based on the AHP method and some quantitative and qualitative criteria were taken into account. The hierarchical structure of the criteria was shown in Fig. 2a. Then, the standard algorithms for the AHP method were performed by the commonly used pair-wise comparison [36]. The evaluations for the pair-wise comparisons of criteria and the final results of selecting the suitable lubricating coatings deposition method from magnetron deposition, cathode-arc deposition and EHDA deposition were presented in the Supporting Information. The priority vectors of the three alternative methods with respect to the criteria and sub-criteria were shown in Fig. 2b. The global priority vectors for the three methods was shown in Fig. 2c. EHDA deposition, with a score of 0.4724, has the highest priority among the three alternative methods. Hence, EHDA deposition, based on the AHP technique, is selected as the method for the deposition of the WS_2/C coatings. 20 μm -thick WS_2/C coatings were deposited onto the tool surfaces with the home-made equipment shown in Fig. 1b. The EHDA process was carried out under ambient temperature and pressure, and its detail was described in [24, 25]. The WS_2 slurry used for deposition was prepared by mixing 0.5 g WS_2 powder (Hunan Huajing Powdery Material Co., Ltd., China), 0.07 g graphite powder (CW-nano Co., Ltd., China), 2.7 g ethanol and 0.1 g ethyl cellulose (AR N20, Greagent). The WS_2/C coated tools of PT, MT-1, MT-2, MT-1-N and MT-2-N were named WPT, WMT-1, WMT-2, WMT-1-N and WMT-2-N, respectively.

2.3 Tests and measurements

Figure 3 illustrated the photo of dry cutting of AISI1045 steel. The geometrical parameters of the dry cutting tools were given by rake angle γ_0 of -5° , clearance angle α_0 of 5° , cutting edge angle κ_r of 45° , edge inclination angle λ_s of 0° and tool corner radius of 0.5. The cutting conditions

Table 1 Mechanical properties of the WC/Co cemented carbide cutting tools

Composition	Density	Flexural strength	Thermal conductivity	Hardness	Fracture toughness	Thermal expansion coefficient
WC + 6wt.% Co	14.6 g/cm ³	2.3 GPa	75.4 W/(m K)	16.0 GPa	14.8 MPa m ^{1/2}	4.5 10 ⁻⁶ /K

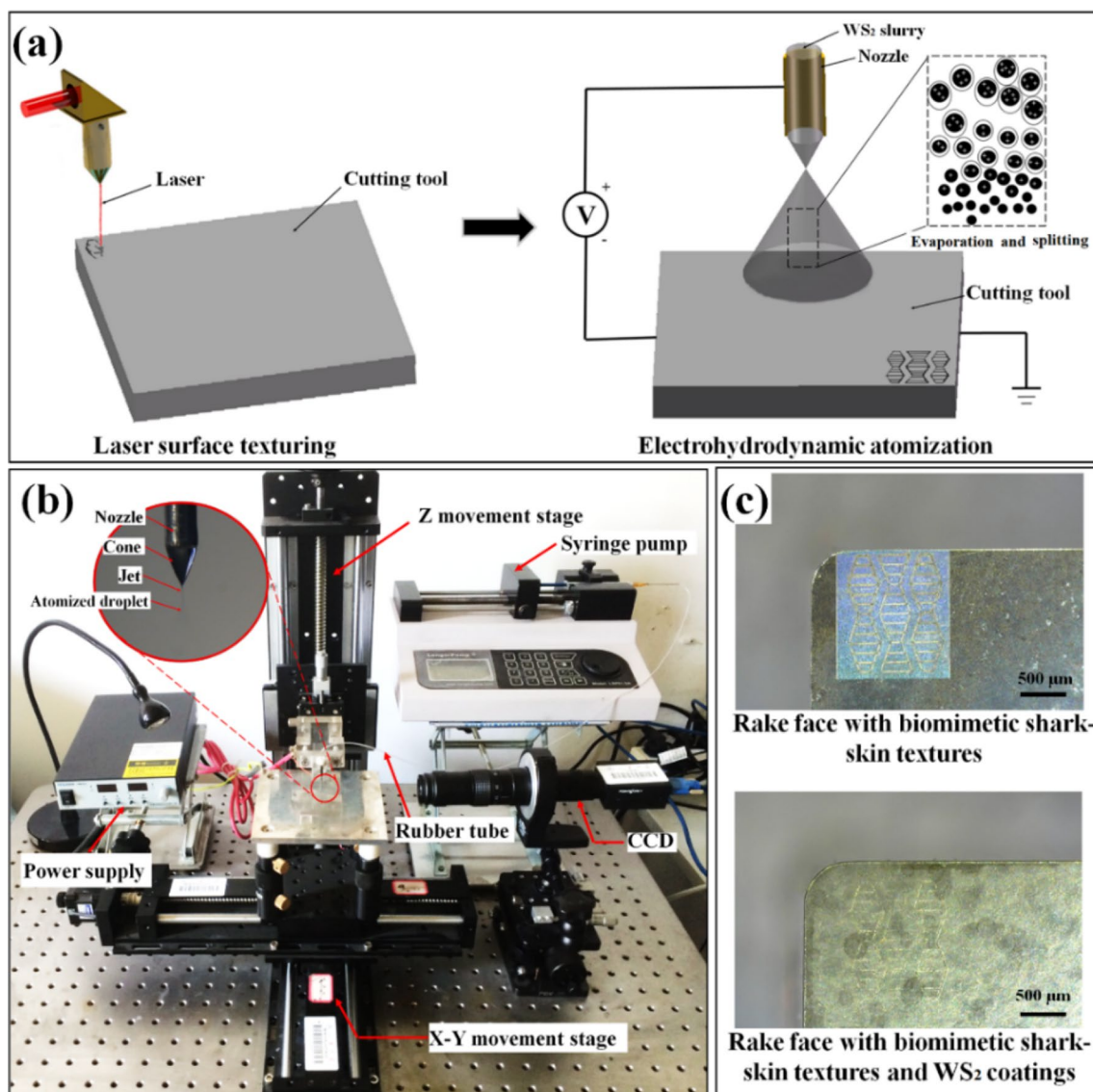


Fig. 1 Schematic drawing of the overall experimental procedure to prepare the dry cutting tools (a). Photograph of the home-made EHDA equipment (b). The rake face with biomimetic shark-skin textures with and without WS₂/C coatings (c)

were shown in Table 3. The temperature profile of the region near to the tooltip was captured by an infrared thermal imager (Fotric 225/226). The cutting forces were measured by piezoelectric dynamometer Kistler 9129AA. The worn tool surfaces were investigated by scanning electron microscope (SEM, QUANTA FEG 250), Raman spectroscopy (Renishaw, United Kingdom) and energy-dispersive X-ray spectroscopy (EDS, QUANTA FEG 250). 3D profiles of the tool surfaces were obtained by a white light interferometer (Wyko NT9300, Veeco Inc., USA). The measurement of the average machined surface roughness R_a was conducted at five different locations by a roughness tester (TR200, JITAIKEYI Inc., China).

3 Results and discussion

3.1 Characteristics of the textures and WS₂/C coatings

As shown in Fig. 4a–c, the shark-skin-inspired surface with rhombuses and ribs structures was fabricated on the rake face of the cutting tool. According to the structural features of shark skin [34], the rhombus structures imitating the shark scales could improve the drag-reducing effect and the grooves imitating the riblet depression structures would help to decrease friction surface and reduce

Table 2 Characteristics of the cutting tools used in this paper

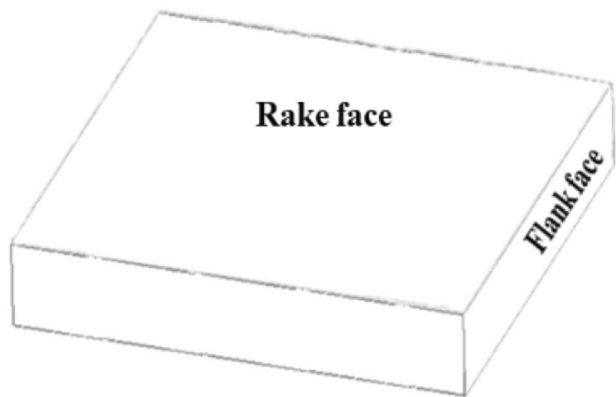
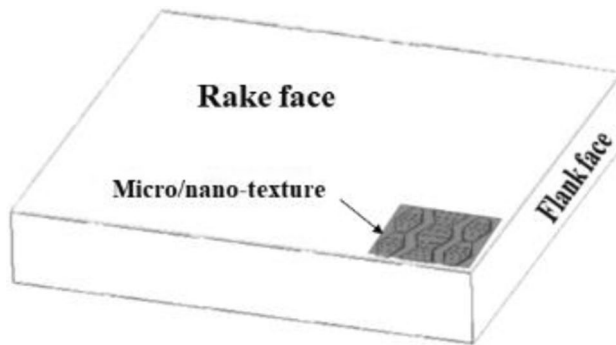
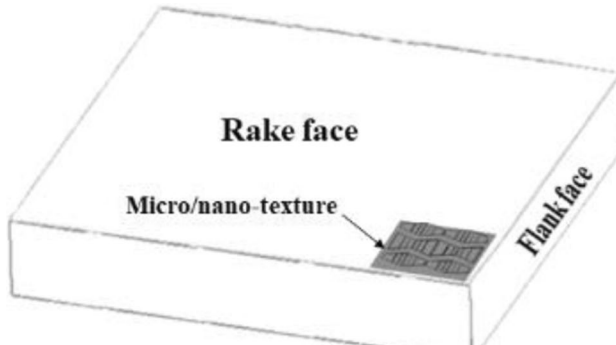
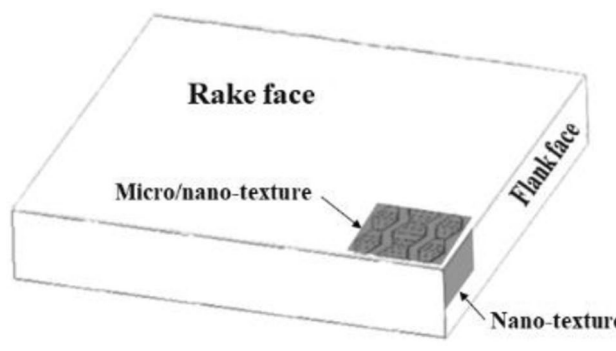
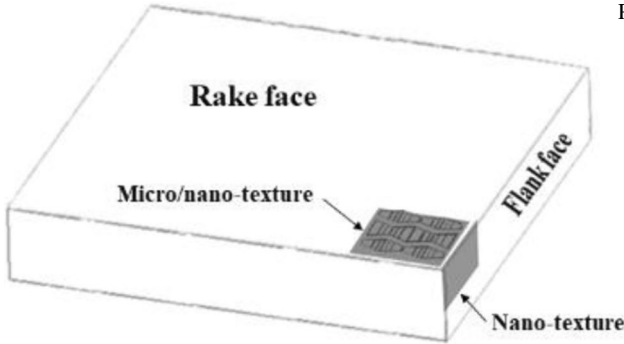
Tool name	Schematic diagram	Description
PT		Polished tool with the surface roughness, Ra less than 80 nm
MT-1		Polished tool with biomimetic shark-skin textures on rake face. The microgroove direction is perpendicular to the main cutting edge
MT-2		Polished tool with biomimetic shark-skin textures on rake face. The microgroove direction is parallel to the main cutting edge
MT-1-N		Polished tool with biomimetic shark-skin textures on rake face and nano-textures on flank face. The microgroove direction is perpendicular to the main cutting edge

Table 2 (continued)

Tool name	Schematic diagram	Description
MT-2-N		Polished tool with biomimetic shark-skin textures on rake face and nano-textures on flank face. The microgroove direction is parallel to the main cutting edge

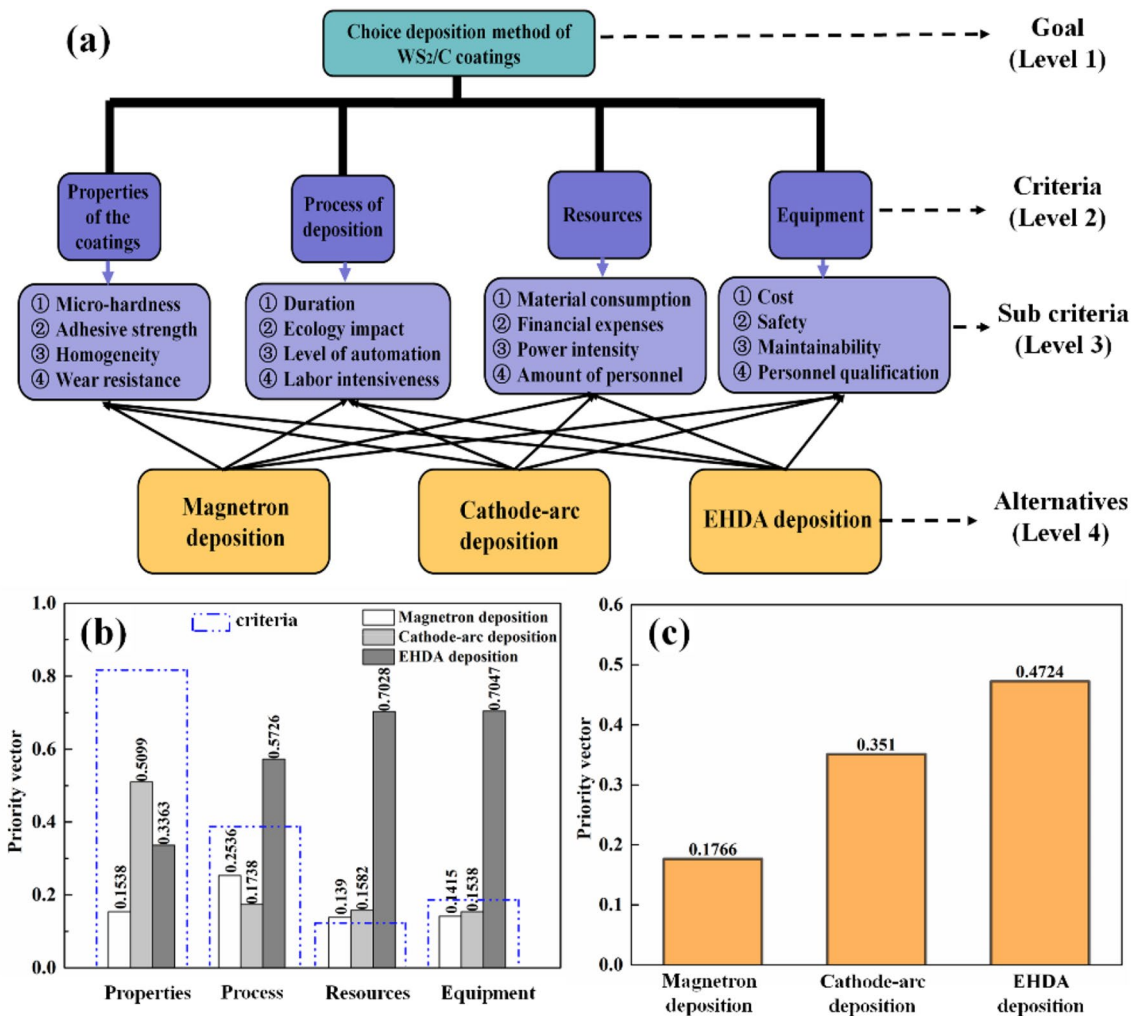
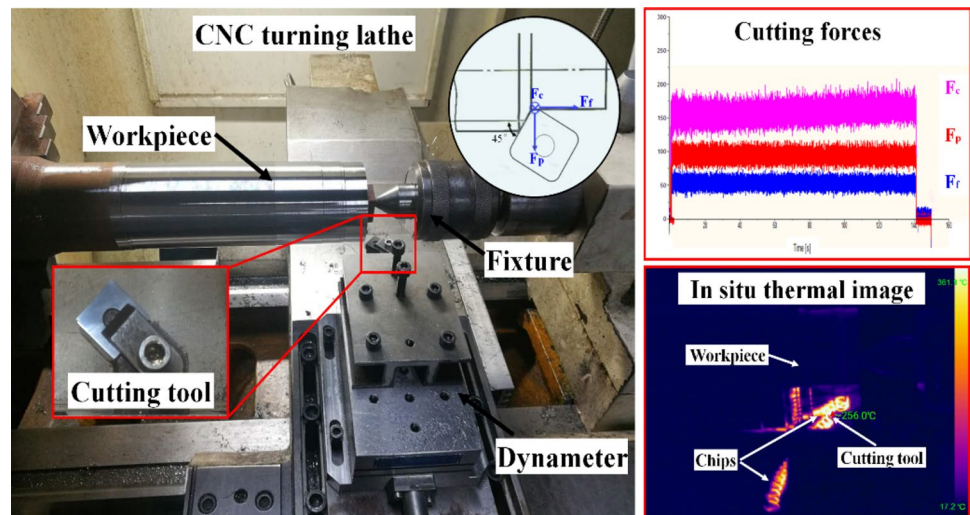


Fig. 2 AHP hierarchical structure for the selection of lubricating coatings deposition methods (a). The efficiency of coatings deposition methods for groups of criteria and sub-criteria (b) and the global priority vectors for three methods (c)

shear stress. Periodic nano-ripples imitating nano-textures of shark skin were fabricated. Their depth and period were ~ 150 nm and ~ 550 nm, respectively according to

author’s previous studies [37]. The profile of one microgroove was shown in Fig. 4e. The depth, aspect ratio and period was ~ 18 μm, ~ 1.8 and ~ 84 μm, respectively.

Fig. 3 Cutting experiments setup**Table 3** Some parameters of the cutting experiment

Feed rate (f)	0.1 mm/r
Depth of cutting (a_p)	0.5 mm
Cutting speed (v)	50, 100, 150, 200 m/min
Workpiece	AISI1045 steel
Cutting tool	Cemented carbide tool YG6
Turning machine	CKD6150H

Figure 5a, b presented the surface micrographs of the WS_2/C coating. The coating presented a dense cluster shape surface, and many particles with different sizes were accumulated. The cross-sectional SEM micrograph, as shown in Figs. 5c, revealed that the particles were two-dimensional ultra-thin sheets. The XRD result (Fig. 5d) showed that the WS_2 coating exhibited a well-developed crystal structure. The diffraction peaks of (002), (004), (100), (103), (006), (110), and (112) corresponded to the crystal planes of hexagonal phase (JCPDS-84-1398). A preferential orientation to basal plane (002) for WS_2 coatings would contribute to its excellent wear resistance and low friction coefficient [38]. The diffraction peak located at 25.6° was (002) carbon crystal plane (JCPDS-75-1621). Figure 5e showed the Raman spectrum of the WS_2/C coating. The peaks located at 351 and 417 cm^{-1} derived from the E_{12g}^1 and A_{1g} vibrational modes of WS_2 [39]. Also, two prominent peaks assigning to the D and G band of carbon were found at 1356 and 1588 cm^{-1} .

3.2 Analysis of dry cutting performance

3.2.1 Cutting force

In this work, the effect of cutting speed on the cutting forces (feed forces F_f , radial thrust forces F_p and tangential forces F_c) for different tools were analyzed. Figure 6 showed the variation of cutting forces with cutting speed. The WMT-2-N tool showed the minimum cutting forces and its feed force F_f , radial thrust force F_p and tangential force F_c was decreased by 36%, 35% and 20%, respectively compared with those of PT tool for the cutting speed of 100 m/min. For the cutting speed of 200 m/min, the reduction of feed force F_f associated with the MT-2-N, WPT and WMT-2-N tool was 14%, 26% and 30%, respectively. For the radial thrust forces F_p , the reduction was 13% for MT-2-N tool, 27% for WPT tool and 34% for WMT-2-N tool. For the tangential forces F_c , the reduction was 7% for MT-2-N tool, 8% for WPT tool and 11% for WMT-2-N tool. These results indicated that the cutting forces reduction achieved by WS_2 -coating the tool may be more effective than that implemented by surface texturing. In the higher cutting speed ranges (> 100 m/min), the cutting force tended to decrease with the increase of cutting speed. The reasons were chiefly as follows: the cutting temperature rose with the increase of cutting speed, which would cause thermal softening and then lead to the decrease of force required for cutting. Depending on the results of cutting forces, the tools of PT, MT-2, MT-2-N, WPT, WMT-2 and WMT-2-N were selected for the follow-up investigations.

3.2.2 Cutting temperature

During the dry cutting process, a lot of energy would be involved for chip removal, which would generate

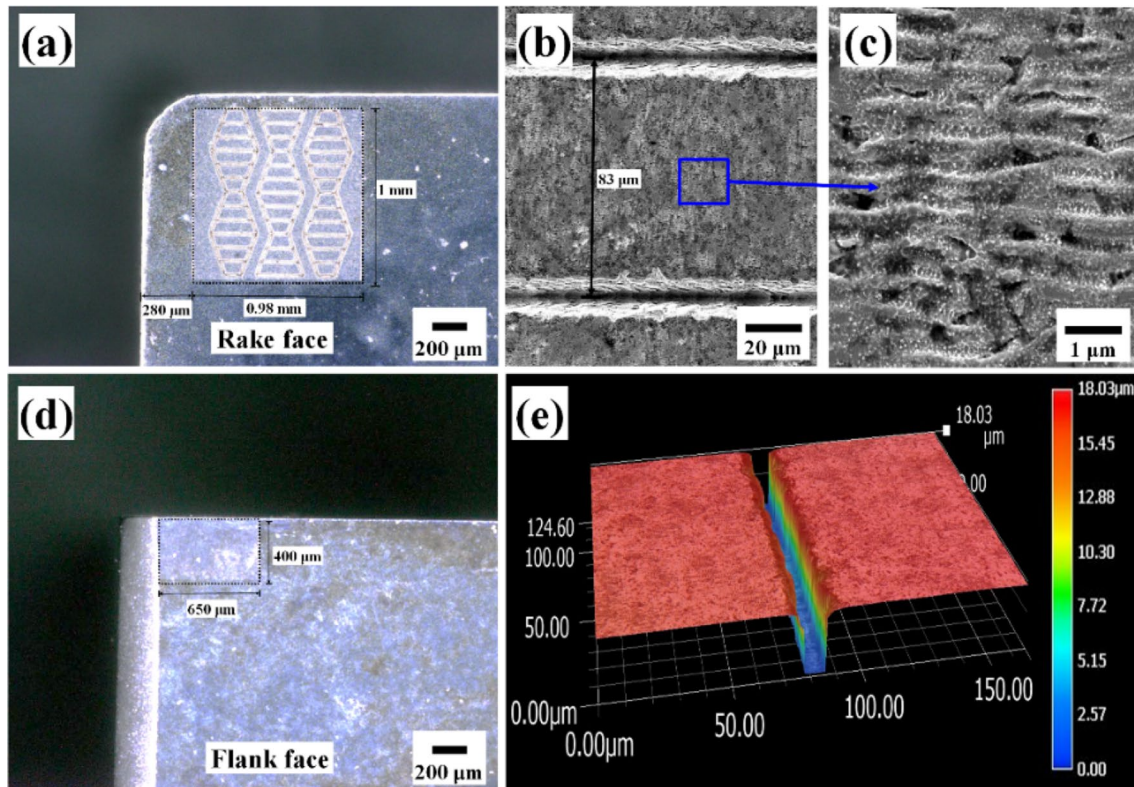


Fig. 4 Characteristics of tool surfaces with shark-skin-inspired structures: rake face with micro/nano-texture (a, b, c); Flank face with nano-texture (d); 3D optical micrographs of one micro-groove (e)

considerable amounts of heat. In this work, the influence of cutting speed on the cutting temperature for different tools was evaluated. Figure 7 showed the variation of cutting temperature with cutting speed for different cutting tools. The cutting temperature of the WMT-2-N tool was minimum at each cutting speed, and the higher cutting temperature was obtained when the cutting speed became higher. In case of the cutting speed of 200 m/min, the highest cutting temperature (~630 °C) was observed for the PT tool and a reduction of 7%, 9% and 10% was obtained for MT-2-N tool, WPT tool and WMT-2-N tool, respectively. Less tool-chip contact area for textured tool effective lubrication after coating WS₂ resulted in lower frictional coefficient and thereby reduced the cutting temperature. The effective heat transfer of textured surface also attributed to the temperature reduction. In the higher cutting speed ranges (> 100 m/min), the cutting temperature of the WMT-2-N tool was decreased by 10–30% in contrast with that of the PT tool.

3.2.3 Friction coefficient of the tool-chip interface

The friction and lubricating behavior of the tool-chip interface would affect tool life, energy consumption of cutting, and machined surface quality. In this work, the friction coefficient μ was obtained from the following equation [40]:

$$\mu = \frac{F_c \sin \gamma_0 + F_f \cos \gamma_0}{F_c \cos \gamma_0 - F_f \sin \gamma_0} \quad (1)$$

The results were illustrated in Fig. 8. The varying trend of the friction coefficients was similar to that of the cutting forces. The largest friction coefficient was achieved at the cutting speed of 100 m/min for the PT tool, and the smallest value was obtained at the cutting speed of 50 m/min for the WMT-2-N tool. An effective reduction in the friction coefficient was observed with the WMT-2-N tool for any given cutting speed. In case of 200 m/min, the reduction of friction coefficient was 7% for MT-2-N tool, 19% for WPT tool and 21% for WMT-2-N tool in contrast with that of the PT tool. So, in order to reducing the friction coefficient between the tool-chip interfaces, the use of WS₂ coating was more effective than that implemented by surface texturing. Textures on the rake face of cutting tool could reduce the tool-chip interface contact length. Moreover, the solid lubricant coating could minimize the friction between the tool-chip interfaces and thereby reduce the heat generated during machining. In the higher cutting speed ranges (> 100 m/min), the friction coefficient tended to decrease with the increase of cutting speed. Such variation could be due to the improved tribological condition of

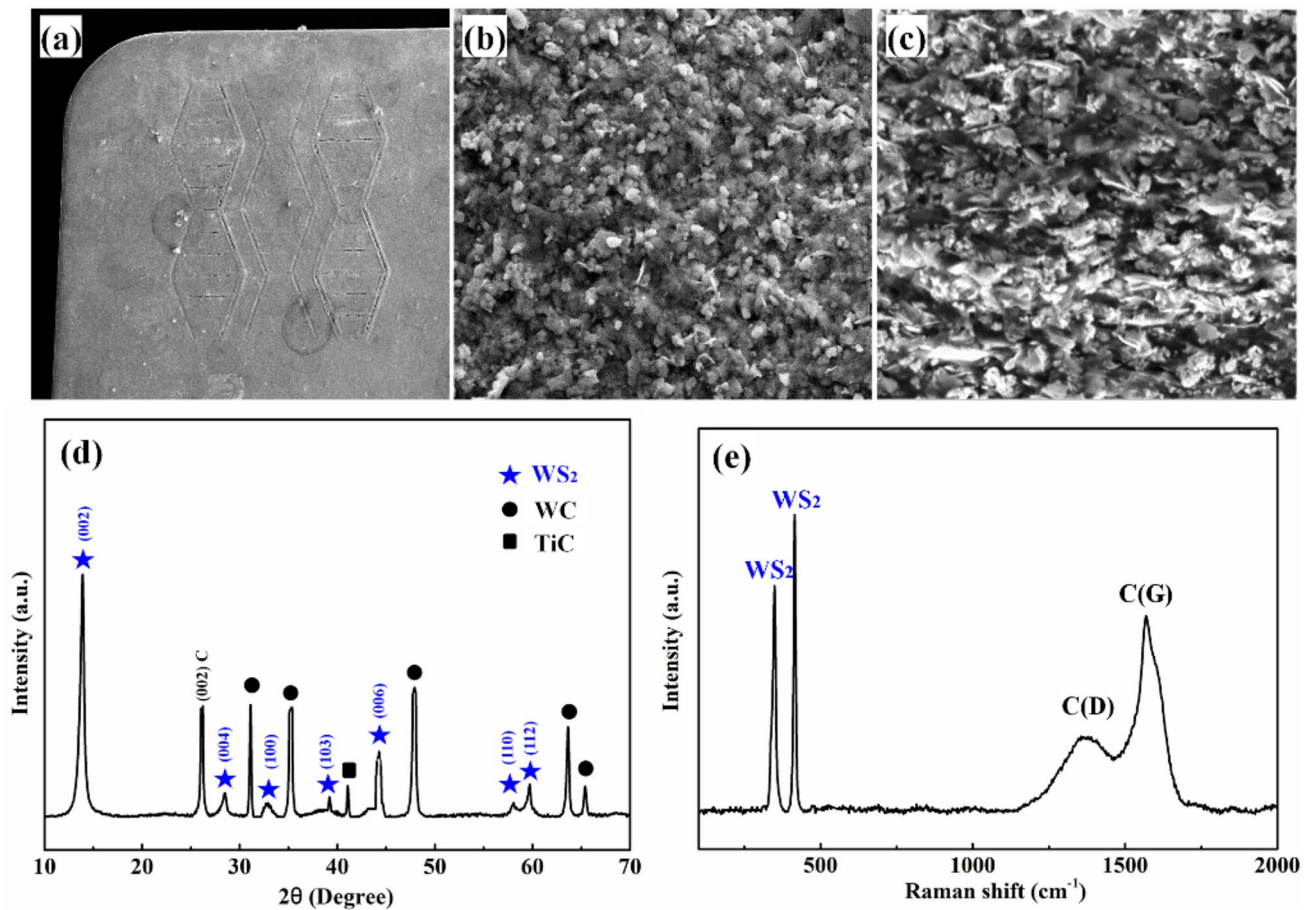


Fig. 5 Characteristics of the WS₂ coatings: surface SEM micrographs (a, b); Cross-sectional SEM micrographs (c); XRD pattern (d) and Raman spectrum (e)

tool-chip interfaces. The high cutting temperatures associated with cutting speed would lead to a thermal softened layer, which could act as solid lubrication.

3.2.4 Shear angle

The shear angle ϕ was obtained by the following equations [41, 42]:

$$\phi = \arctan \frac{\cos \gamma_0}{\xi - \sin \gamma_0}, \quad \xi = \frac{a_{ch}}{a_{cp}} \quad (2)$$

Figure 9 showed the shear angle variation with cutting speed. An increase of shear angle was observed when the cutting speed rose. This is principally because the chip thickness reduced as the cutting speed rose, which increased chip thickness ratio and consequently increased the shear angle. As shown in Fig. 9, the influence of cutting speed on the shear angle for PT tool (17%) is a little greater than that for the WMT-2-N tool (10%). While for the constant cutting speed, the WMT-2-N tool had a higher shear angle,

increasing by 73–85% compared with that of the PT tool. The texture on the rake face could affect the chip thickness ratio and thereby the shear angle, as the formation of chips involved the shearing of the workpiece material in a plane extending from the tool edge to the position where the chip leaves the work surface. The tool-chip contact was referred as a tribological contact. For the PT tool, the severe friction was there and due to the frictional effect, chip thickness was large. With the introduction of textures and lubricant coatings, the increase in shear angle is facilitated by the ease of chip flow over the rake face due to reduced friction. Furthermore, the application of textures and WS₂ coatings on the cutting tool will reduce the adhesion of chip material on the cutting tool surface, which would be helpful for chip flow. For the cutting speed of 200 m/min, the shear angle was found to be 19° for PT tool, 22° for MT-2-N tool, 28.1° for WPT tool and 33° for WMT-2-N tool. The lubricant coatings were more effective than textures in increasing the shear angle. The greater shear angle can contribute to lower cutting heat, lower specific shearing energy and lower power requirements [43].

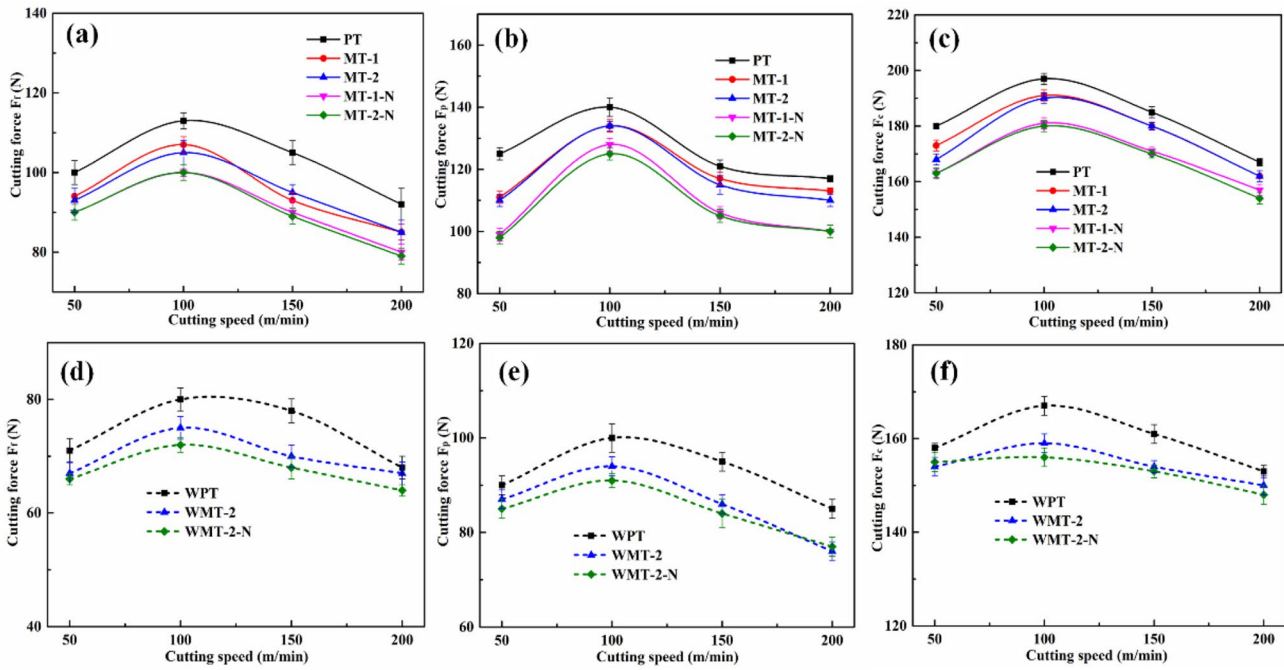
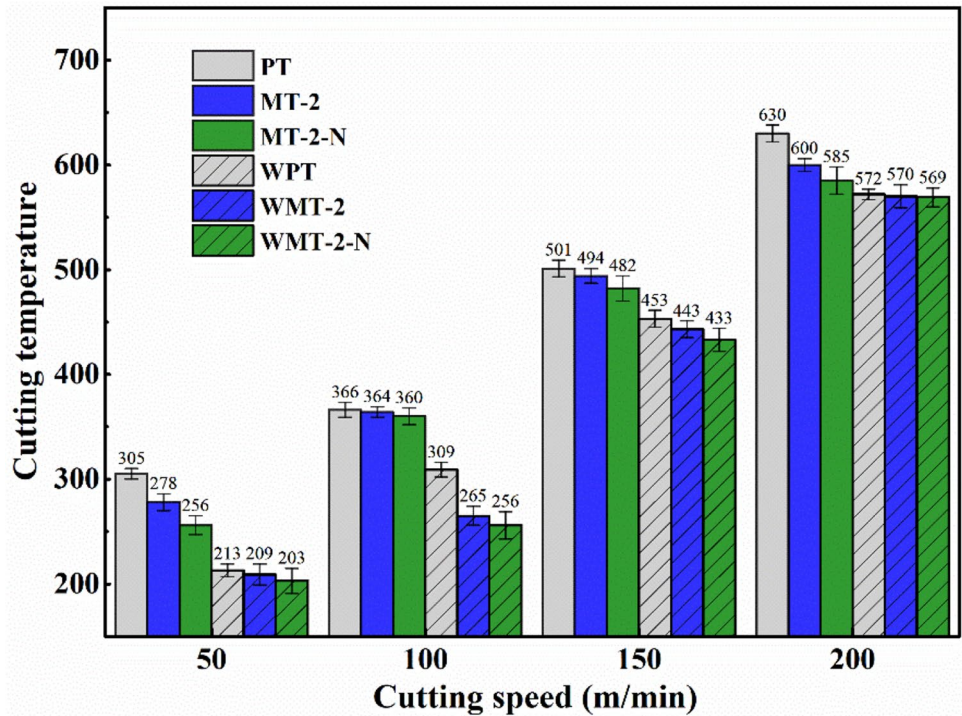


Fig. 6 Variation of cutting forces with cutting speed: feed forces (a, d); Radial thrust forces (b, e); Tangential forces (c, f)

Fig. 7 Variation of cutting temperature with cutting speed



3.2.5 Specific cutting energy

Specific cutting energy (SCE), characterizing the energy consumption of removing the workpiece materials, was obtained by the equation:

$$SCE = \frac{F_c}{f \cdot a_p} \tag{3}$$

Figure 10 showed the SCE results of all tools with respect to different cutting speeds. The maximum SCE

Fig. 8 Friction coefficient of the tool-chip interfaces for different tools

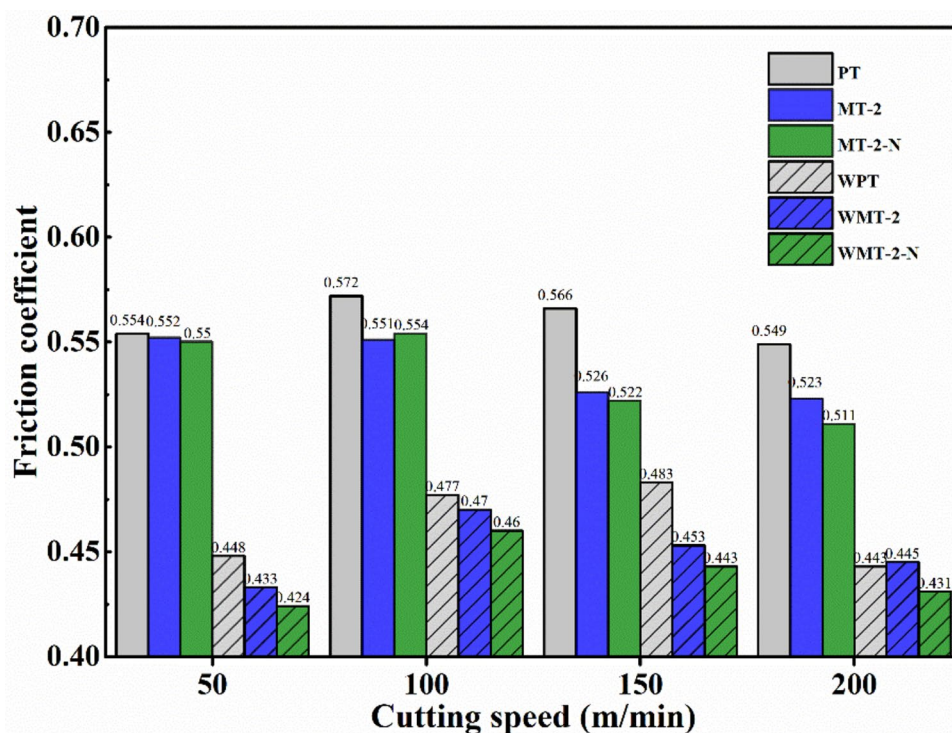
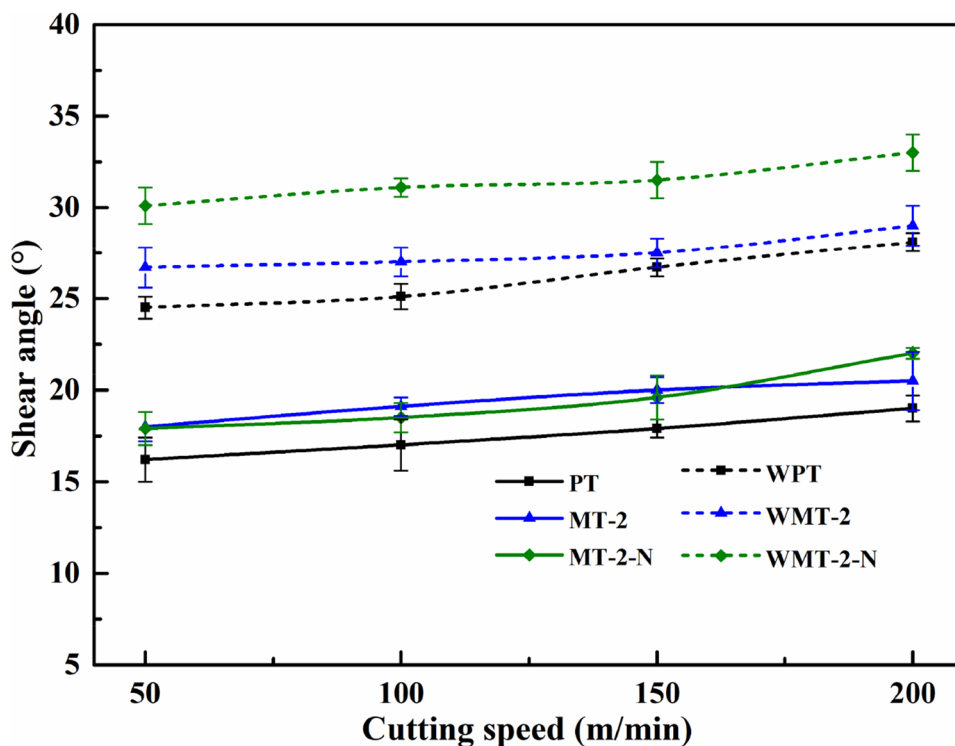


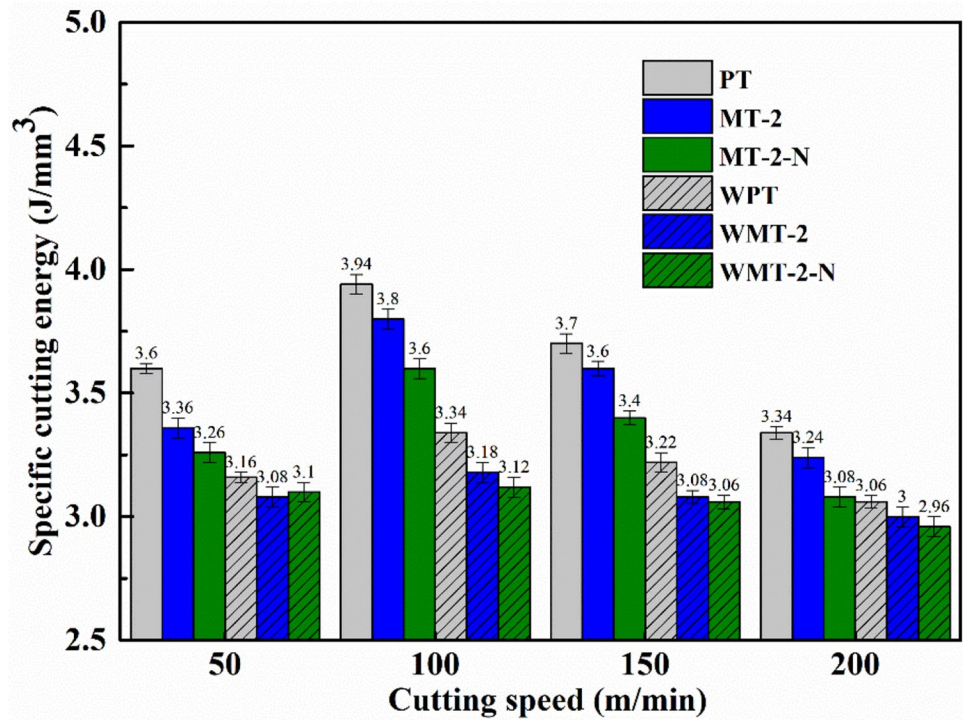
Fig. 9 Shear angle of different tools at different cutting speeds



was achieved for PT tool when cutting speed was 100 m/min, which was about 3.94 J/mm³. A reduction of SCE value with the order of 3–15% was observed as the cutting speed rose from 100 to 200 m/min. In case of a constant cutting speed, the SCE reduction associated with the

WMT-2-N tool was 11–20% compared with the PT tool. Cutting energy reduction can be attributed to the reduction of cutting forces.

Fig. 10 Specific cutting energy of different tools

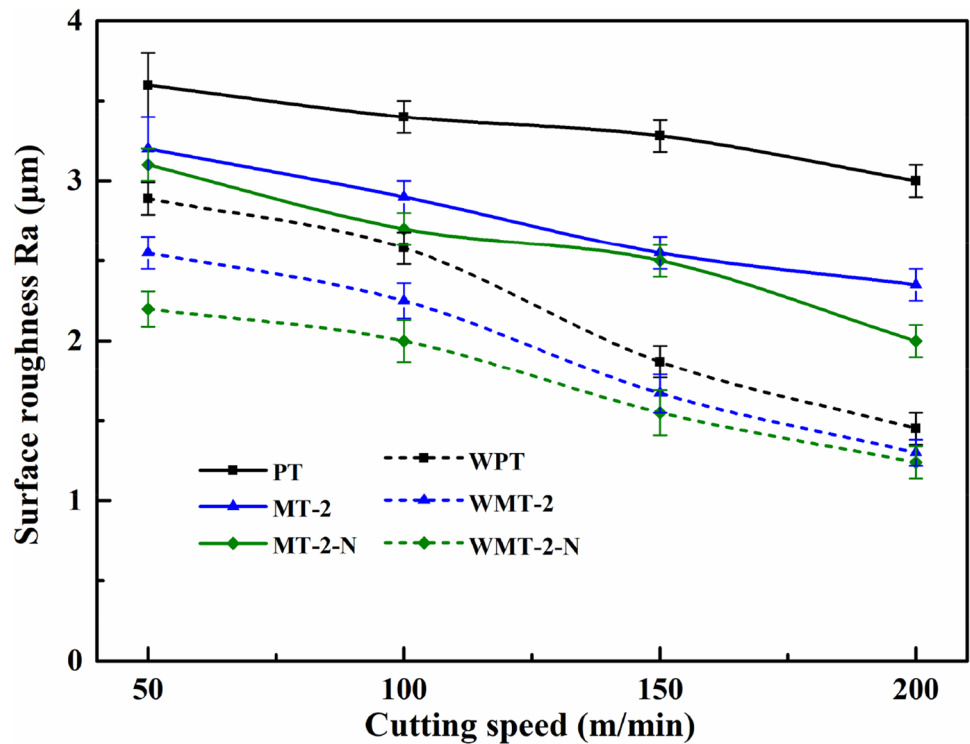


3.2.6 Machined surface roughness

The machined surface roughness Ra of the workpiece was measured and presented in Fig. 11. An increase of cutting speed lead to the decrease of surface roughness Ra, which

was well consistent with some literature review [44, 45]. When the cutting speed was 200 m/min, the surface roughness Ra was high (~3.6 μm) in case of PT tool, while low (~1.2 μm) for the WMT-2-N tool. In the dry cutting condition, the PT tool may be exposed to high cutting temperature

Fig. 11 Variation of machined surface roughness Ra with cutting speed



and contact stress, which would lead to some surface defects like abrasive marks, wear debris and adhering layers, and consequently to deterioration of the machined surface. For the WMT-2-N tool, the lubrication action of WS_2/C coatings and textures prevented the temperature rising and hence reduced the thermal damage for deteriorating machined surface finish.

3.3 Analysis of tool wear

3.3.1 Tool life

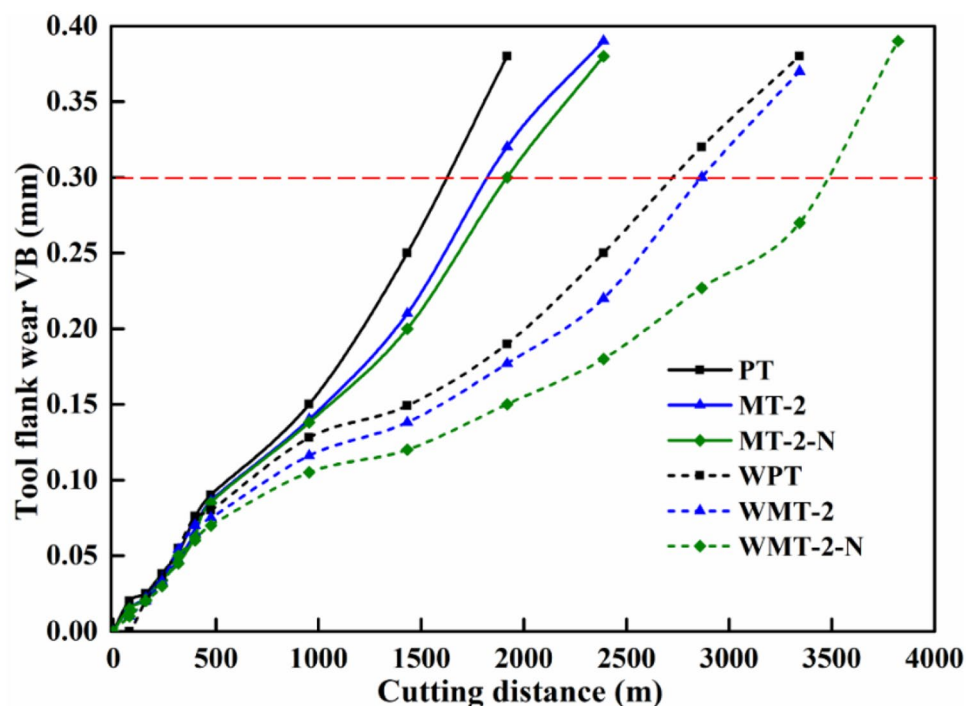
Figure 12 showed the change of tool flank wear VB with the increase of cutting distance at the cutting parameters: $v=200$ m/min, $f=0.1$ mm/r and $a_p=0.5$ mm. Every date was obtained by averaging three repeated experimental results under the same test conditions. For all tools, under the given cutting parameters, there were three wear stages: initial break-in stage, steady wear stage and sharp wear stage. In the initial break-in stage, due to the high pressure stress caused in the narrow contact area between the tool and the workpiece, rapid abrasive wear was produced. The initial break-in stage of all tools lasted about ~ 500 m. In the steady wear stage, the wear rate slowed down because of the increase of the contact area between the tool and the workpiece. The longer steady wear stage tools have, the longer reliability duration of cutting they have. Form Fig. 12, the tools configured with shark-skin-inspired structures or/and WS_2/C coatings showed longer steady wear stage with a slow and stable rising wear rate. The sharp wear stage of all

tools has almost the same characteristics. The tool life criteria was as follows: the average tool flank wear $VB > 0.3$ mm, depending on ISO standard 3685. The tool life of MT-2-N and WPT was improved by 17.7% and 69.3%, respectively, compared with that of PT tool, indicating that the tool life improvement achieved by WS_2 -coating the tool may be more effective than that implemented by surface texturing. The maximum value obtained in the WMT-2-N tool was ~ 3486 m, which was 2.1 times longer than that of the PT tool. The significant improvement of tool wear life may be linked closely to the improvement of the tribological state at the tool-workpiece contact zone. In general, the combination of surface texturing and deposited WS_2/C coatings is a suitable method to increase tool life.

3.3.2 Flank wear characteristics

Figure 13 showed the worn flank surface morphologies of PT, WPT, MT-2-N and WMT-2-N tools with the cutting distance of 1061 m under the cutting parameters: $v=200$ m/min, $f=0.1$ mm/r and $a_p=0.5$ mm. Some abrasive marks were formed on the flank face of the PT tool (Fig. 13a), indicating its abrasive wear. The formation of abrasive marks was mainly due to the increase of friction between tool surface and workpiece surface, which was caused by the hard particles from workpiece, built-up layer and chips. In addition, serious adhesion phenomenon, including built-up edge and adhering layers, was found. Compared with the unworn area (point A2), the content of Fe and O elements were enhanced significantly on point A1 of tool flank face.

Fig. 12 Tool flank wear curves of different tools ($v=200$ m/min, $f=0.1$ mm/r and $a_p=0.5$ mm)



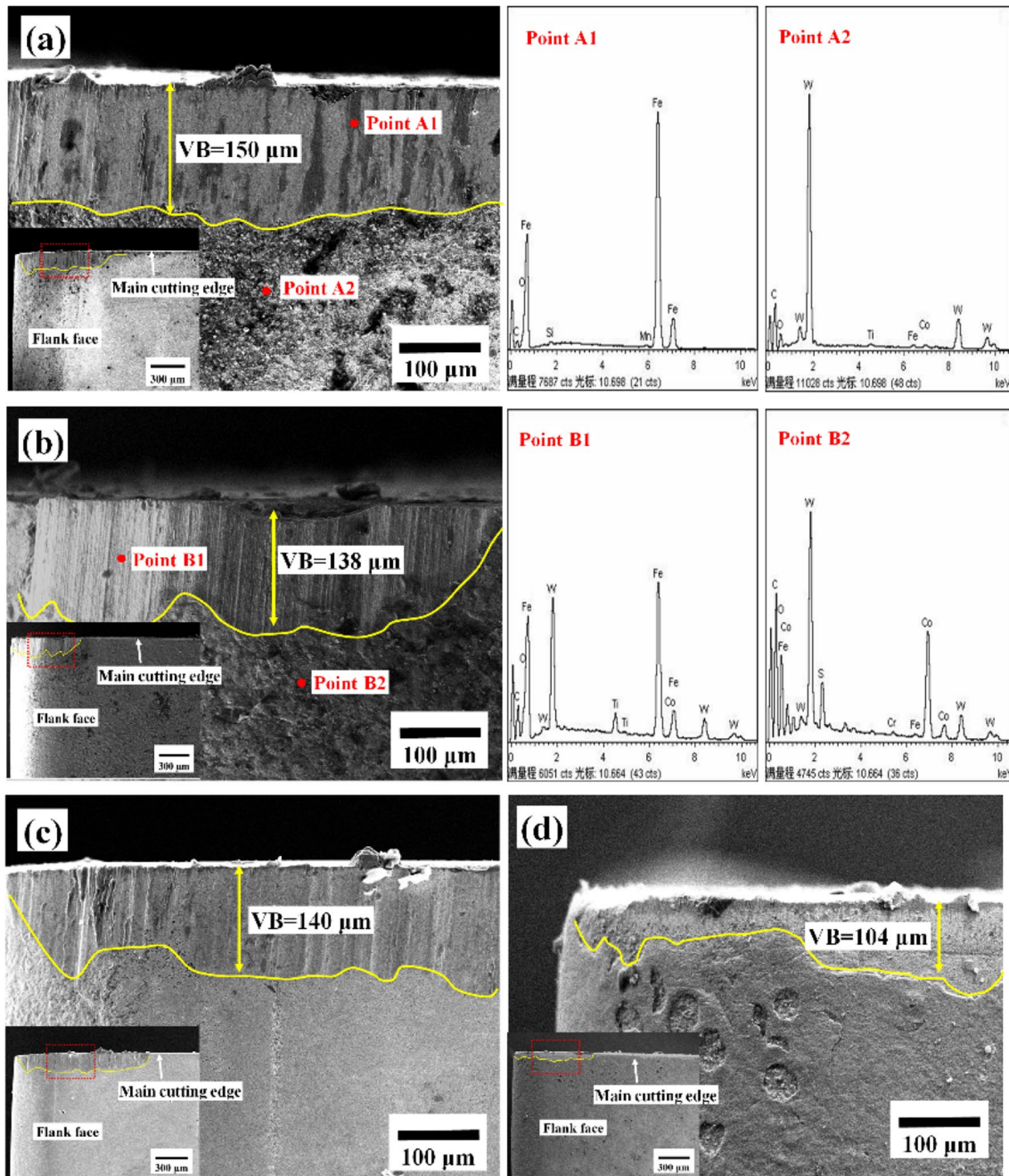


Fig. 13 Flank wear morphologies of different tools: PT (a); WPT (b); MT-2-N (c); WMT-2-N (d); ($v=200$ m/min, $f=0.1$ mm/r, $a_p=0.5$ mm and cutting distance = 1061 m)

This indicated that the adhering layer was oxidized under the high cutting temperature (~ 630 °C). So the main flank wear mechanism in dry cutting AISI1045 steel was abrasive wear and adhesive wear. After depositing WS_2 coating (Fig. 13b), the adhesive wear became slight and no built-up edge was formed, which was well consistent with the low tool flank wear value of the corresponding varying curve shown in Fig. 12. For the MT-2-N tool (Fig. 13c), the flank face was worn relatively uniformly, while some built-up edge and

adhesion but no notch were formed. The WMT-2-N tool (Fig. 13d) exhibited the best anti-wear ability in contrast with other tools.

3.3.3 Rake wear characteristics

The rake wear was mainly caused by the physical and chemical reaction between the chip material and the cutting tool material. Figure 14 exhibited the worn rake surface

morphologies of PT tool with the cutting distance of 1061 m under the cutting parameters: $v=200$ m/min, $f=0.1$ mm/r and $a_p=0.5$ mm. The morphology results suggested that many wear debris were distributed on the worn face. In the machining zone near the main cutting edge (Fig. 14c), due to the elevated temperature and high contact pressure, the wear debris got stuck onto the tool surface and caused the adhering layer and built-up edge. The further composition analysis of the adhering layer by the Raman spectrum (Fig. 14d) showed that Fe_2O_3 was detectable. Also, some abrasive marks were observed on the worn face. Generally, the main rake wear type of PT tool was adhesive and abrasive wear. Figure 15 showed the worn rake faces of MT-2-N tool with biomimetic shark-skin structure, and its wear degree became milder. In the region near the main cutting edge, an adhering layer composed of Fe_3O_4 and Fe_2O_3 was formed (Fig. 15a, d). At the textured area, the well-distributed rhombus cells would help to reduce the shear stress during the dry cutting process and the micro-grooves inserted in the rhombus cells had a significant effect on reducing the contact area, all of

which would improve the lubricating effect of machining process [46]. Owing to the high contact pressure, lots of wear debris were pressed into the micro-grooves (Fig. 15b, c), which would effectively alleviate the abrasive wear.

Figure 16 exhibited the rake wear morphologies of the WPT tool. In the machining zone, the WS_2/C coating was peeled away and the adhering layer and built-up edge were formed (Fig. 16d, e), which could be confirmed by the EDS map of Fe and S element (Fig. 16b, c). Fe_3O_4 , Fe_2O_3 , WS_2 and its oxidized products (WO_3), some sulfate and sulphide ($FeSO_4$ and FeS) were detected from the wear debris by Raman spectrum (Fig. 16f). These results indicated that WS_2/C coating deposited on the polished tool surface could not play a long-time lubricating role. Its premature failure would make the tool substrate directly contact with the workpiece, which would lead to severe tool wear. For the WMT-2-N tool, when the microgrooves were penetrated by wear debris, the WS_2/C particles stored within the grooves would be squeezed out and then began its function in reducing the friction between workpiece and

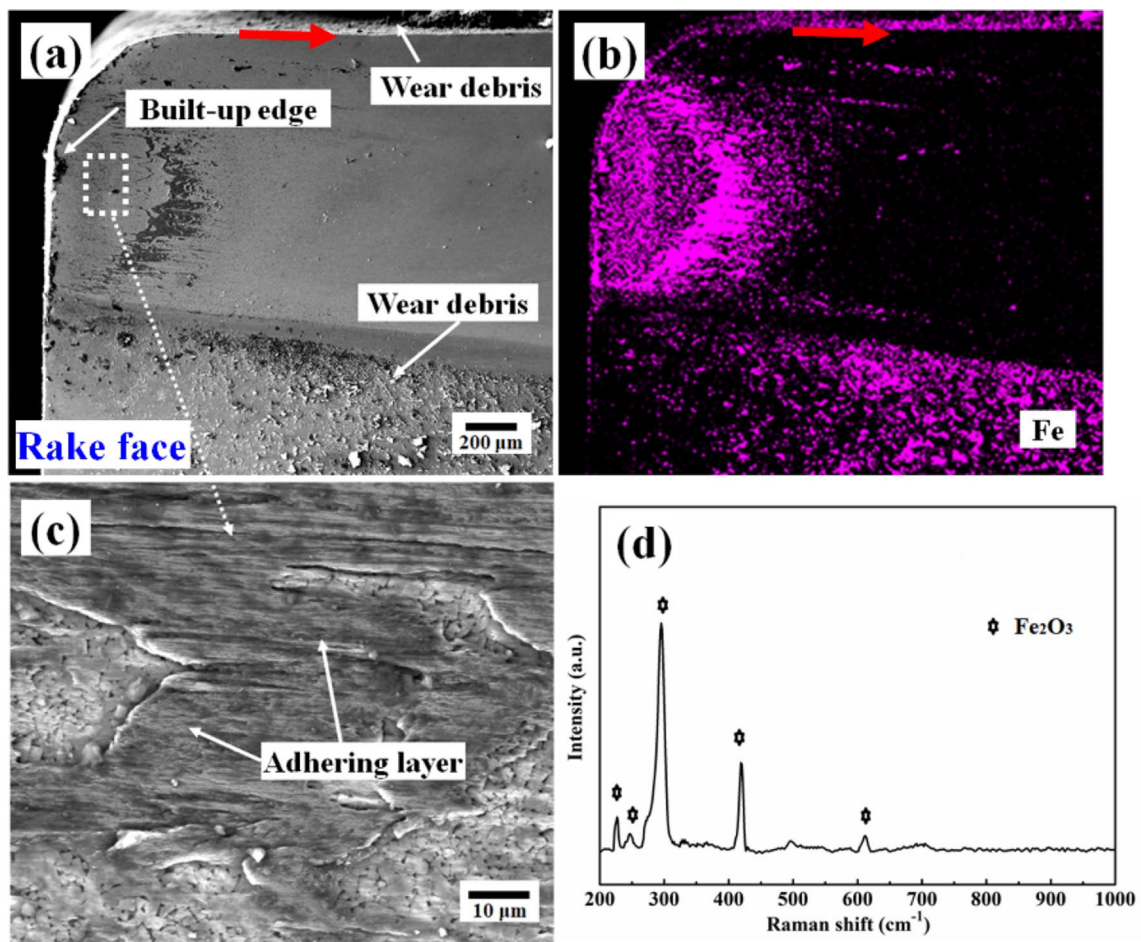


Fig. 14 Rake wear morphologies of the PT tool (a, c) and EDS map of Fe element (b). Raman spectrum of the adhering layer (d). ($v=200$ m/min, $f=0.1$ mm/r, $a_p=0.5$ mm and cutting distance = 1061 m; the red arrow shows the direction of chip flow)

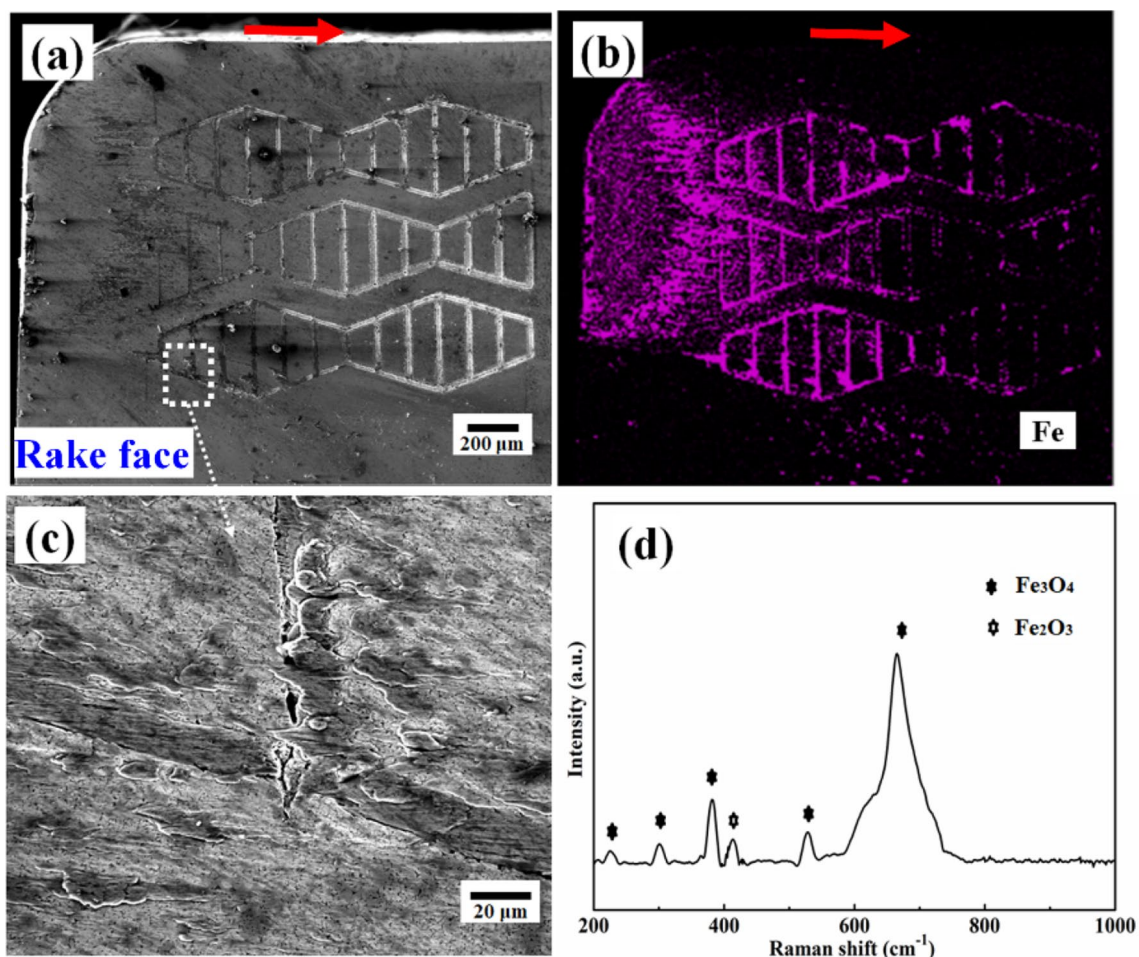


Fig. 15 Rake wear morphologies of the WMT-2-N tool (a, c) and EDS map of Fe element (b). Raman spectrum of the adhering layer (d). ($v=200$ m/min, $f=0.1$ mm/r, $a_p=0.5$ mm and cutting distance = 1061 m; the red arrow shows the direction of chip flow)

tool. As seen in Fig. 17a, c, the amount of WS_2/C particles retained on the textured surface was higher compared with that of the polished tool surfaces. Therefore, a longer period of lubrication can be obtained. In addition, benefiting from the storage function of grooves (Fig. 17b, e), the scratching distance of wear debris on the tool surface was reduced. As a result, the damage of the cutting tool was reduced and the tool life was increased. Raman spectroscopic analysis for the wear debris showed the prominent peaks of WS_2 as well as a few Fe_3O_4 (Fig. 17f).

Figure 18 showed the 3D micrographs and surface profiles of rake faces for different tools. A large crater with a depth of ~ 2.5 μm was found on the worn rake face of the PT tool, indicating its severe abrasive wear. The shallow and narrow abrasion craters were observed on the worn rake face of MT-2-N and WPT tools, and their depth had no noticeable difference. WMT-2-N tool showed the minimal abrasive wear.

3.4 Sustainability assessment

Sustainability assessment for the dry cutting process needs to focus not only on the product, but also on the manufacturing process involved. This assessment needs some metrics based on both product and manufacturing processes. In this work, measures for the evaluation were:

- Energy consumption;
- Manufacturing cost;
- Process performance;
- Machined surface quality;
- Environmental effect;
- Waste production and disposal;
- Operator health and safety.

Taking influencing factors of energy consumption, manufacturing cost, machined surface roughness, workpiece

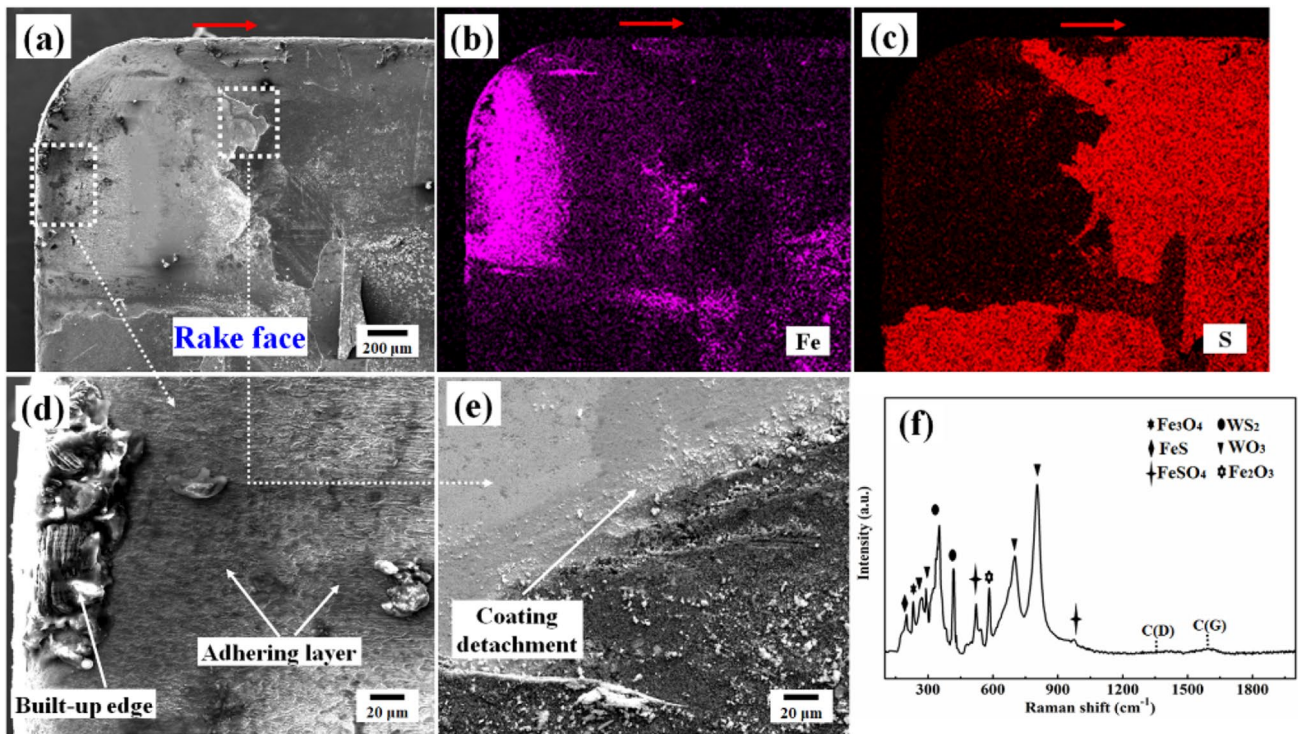


Fig. 16 Rake wear morphologies of the WPT tool (a, d, e). The EDS map of Fe element (b) and S element (c). Raman spectrum of the wear debris (f). ($v = 200$ m/min, $f = 0.1$ mm/r, $a_p = 0.5$ mm and cutting distance = 1061 m; the red arrow shows the direction of chip flow)

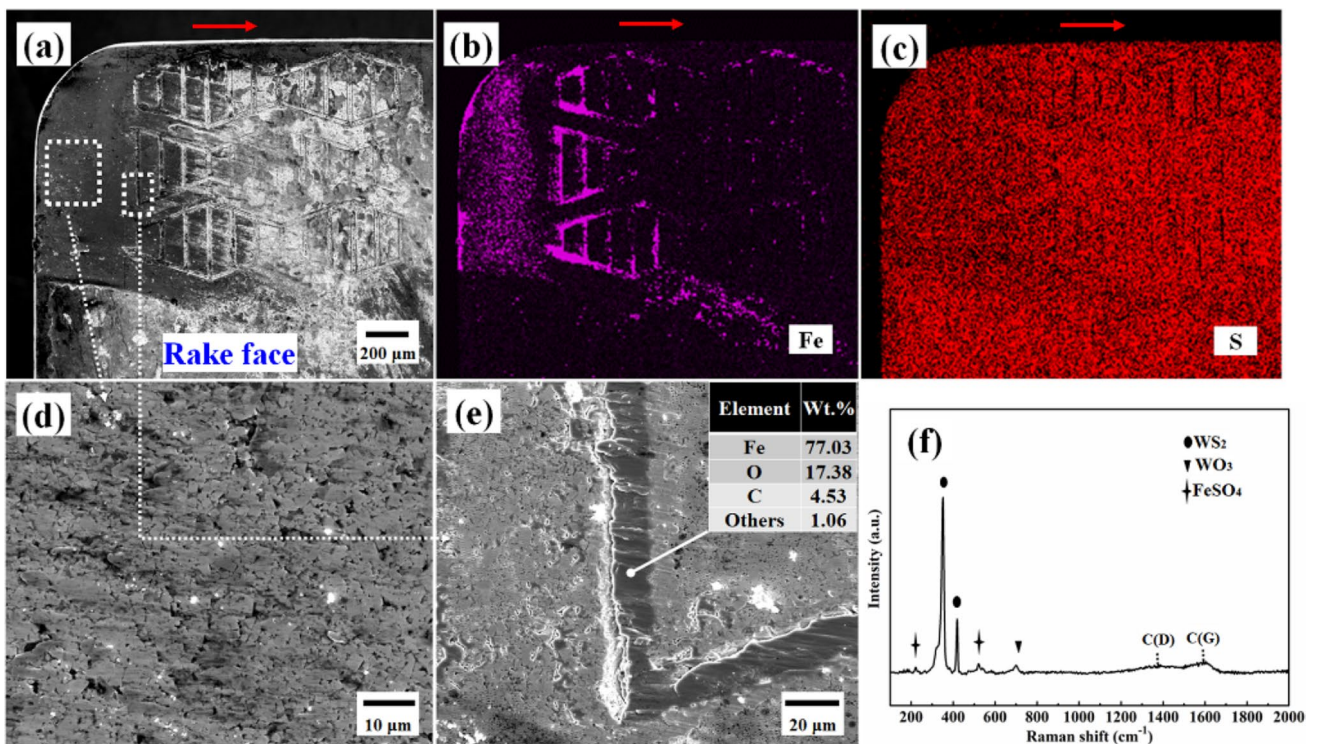


Fig. 17 Rake wear morphologies of the WMT-2-N tool (a, d, e). The EDS map of Fe element (b) and S element (c). Raman spectrum of the wear debris (f). ($v = 200$ m/min, $f = 0.1$ mm/r, $a_p = 0.5$ mm and cutting distance = 1061 m; the red arrow shows the direction of chip flow)

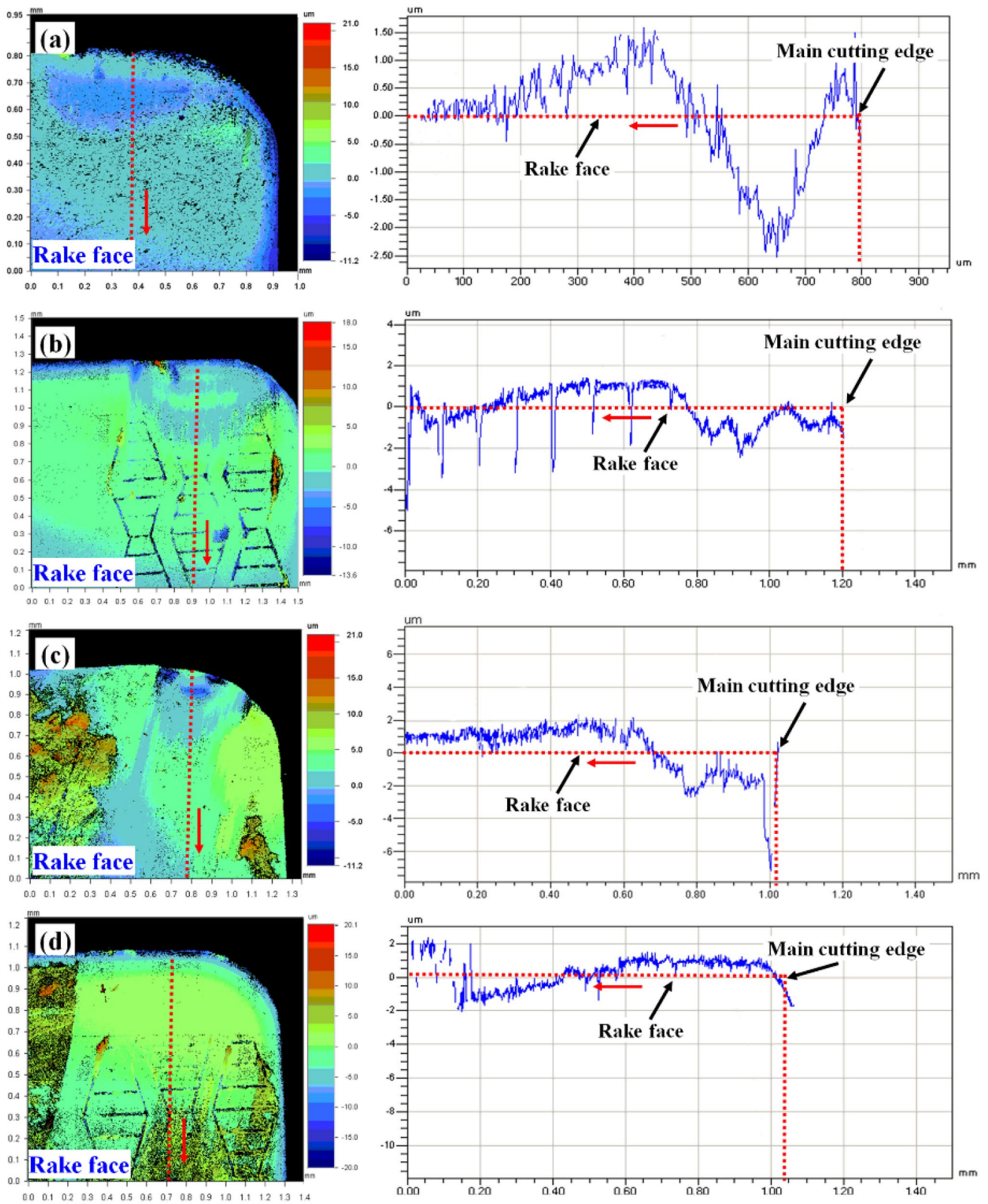


Fig. 18. 3D micrographs and surface profiles of rake face after dry cutting: PT (a); MT-2-N (b); WPT (c); WMT-2-N. ($v=200$ m/min, $f=0.1$ mm/r, $a_p=0.5$ mm and cutting distance = 1061 m; the red arrow shows the direction of chip flow)

cleaning, scrap disposal, environmental effect, and operator health and safety into account, the calculation of product sustainability index (PSI) was carried out. The scoring criteria for each influencing factor were represented in Fig. 19. In the process of sustainability assessment, the scores of all influencing factors were allotted from poor to excellent, then the PSI for dry cutting AISI1045 steel was obtained by adding the scores of all influencing factors, as shown in the following the equation:

$$PSI = \frac{\sum_{i=1}^n IF_i}{n \cdot 10} \cdot 100\% \tag{4}$$

where n is the number of the influencing factors and IF is the score of the influencing factor. It should be noted that the sustainability assessment was carried out in our laboratory environment, unlike the actual industrial condition, some aspects like electricity cost, workpiece cost, labor cost, etc. were ignored in order to simplify the process. Due to the limitation of measuring means, only the surface roughness Ra was considered when scoring the machined surface quality. The detailed description of the scoring process for each influencing factor was presented below.

Energy consumption: to estimate the energy consumption (E) of dry cutting AISI1045 steel using different cutting

tools, the lathe power (P_l) and energy use of coating (E_c) and texturing (E_t) were considered. P_l can be calculated by the following equation [47, 48]:

$$P_l = \frac{F_c \cdot v}{60 \cdot \omega} \tag{5}$$

where F_c and v is the tangential force and cutting speed, respectively. ω is the transmission efficiency of the lathe (0.75). The values of E_c and E_t were calculated as the sum of energy consumed by each component

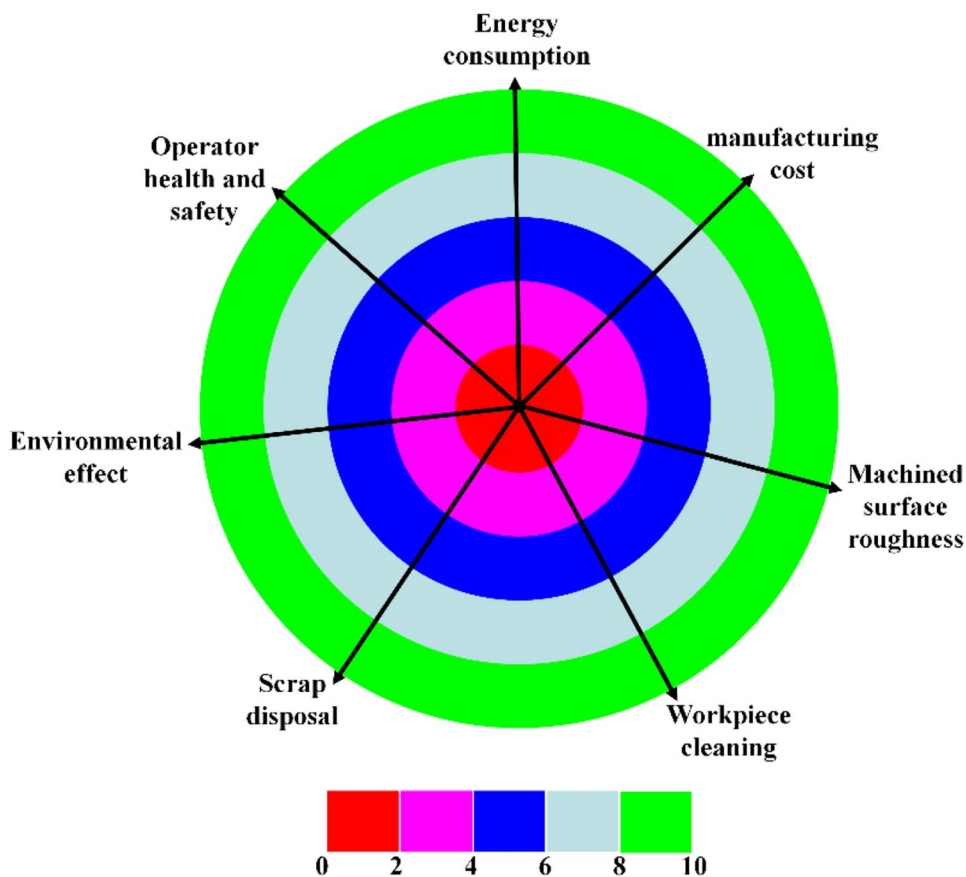
$$E_c/E_t = \sum_{i=1}^n P_i \cdot t_i \tag{6}$$

where P_i is the powder demand of device (heater, X–Y moving platform, pump, laser, etc.) and t_i is the operating time. Then, the energy consumption E was calculated by the following formula:

$$E = P_l \cdot t + E_c + E_t \tag{7}$$

From the Eq. (5), the energy consumption of the lathe using PT, MT-2, MT-2-N, WPT, WMT-2 and WMT-2-N was 7.9 MJ, 7.8 MJ, 6.8 MJ, 6.8 MJ, 6.5 MJ and 5.6 MJ, respectively. The cutting conditions are: $v = 200$ m/min, $f = 0.1$ mm/r, $a_p = 0.5$ mm and cutting time = 5 min. The

Fig. 19 Scoring criteria for each influencing factor during the sustainability evaluation



energy consumption of coating was 1.7 MJ, and the energy consumption of texturing with ns laser and fs laser was 0.6 and 1 MJ, respectively. Depending the Eq. (7), the energy consumption of dry cutting AISI1045 steel using PT, MT-2, MT-2-N, WPT, WMT-2 and WMT-2-N was 7.9 MJ, 8.4 MJ, 8.4 MJ, 8.5 MJ, 8.8 MJ and 8.8 MJ, respectively. Thus, a score of “7” was provided to WMT-2-N and WMT-2, “7.2” to WPT, “7.4” was assigned to MT-2 and MT-2-N, and “7.9” in case of PT.

Manufacturing cost: this aspect was scored through tool cost, tool life and MRR. Then the total score of manufacturing cost was obtained by summing up the three scores. WMT-2-N tool has the highest tool cost, as it needed to add lubricating coatings and textures. However, the good lubrication of WMT-2-N leads to longer tool life and decreased its manufacturing cost. The higher MRR would cause higher productivity and lower manufacturing cost.

Machined surface roughness: the score of machined surface quality was determined according to the Machined surface roughness Ra. A low surface roughness means a good surface quality and will get a high score.

Workpiece cleaning: there is no need to clean the workpiece in our case of dry cutting, thus a high score of “10” was assigned to all experimental conditions.

Scrap disposal: the chips were formed during the cutting process. Under the dry cutting condition, the chips were free from the cutting fluid and easy to be handled or stored. So a high score of “9” was given.

Environmental effect: dry cutting can protect the environment from being harmed by cutting fluid. The content of PM2.5 solid particles produced in the machining zone was not distinct significantly for all tools. However, the noise level decreased with the improved tribological property of tool. The process of coating and laser texturing would generate emissions, polluting the environment. Thus, a score of “9” was provided to WMT-2-N, “8” to WPT and WMT-2, “7” to MT-2 and MT-2-N, and “6.5” in case of PT.

Operator health and safety: in the dry cutting condition, the operator health and safety were free from the harm of cutting fluid. While the cutting temperature of the PT tool was very high which caused the increased temperature of the

machined products and would increase the operational risk when exposed to the high-temperature component. At the same time, the noise level of the PT tool was highest among all tools due to the high cutting force and poor lubrication condition. Thus, a score of “9” was provided to WMT-2-N, “8” to WPT and WMT-2, “6” was assigned to MT-2 and MT-2-N, and “5” in case of PT.

The appropriate scores of all considered aspects were given (see Table 4) and the total PSI was determined, as represented in Fig. 20. The condition which got a higher score of PSI would more easily achieve sustainable manufacturing. As was shown in Fig. 20, the highest total PSI of 77.1% was obtained in case of the dry cutting experiment using WMT-2-N tools. That is, dry cutting AISI1045 steel using WMT-2-N tools was practically viable in terms of sustainability, which would provide better economic, social and environmental benefits.

4 Conclusions

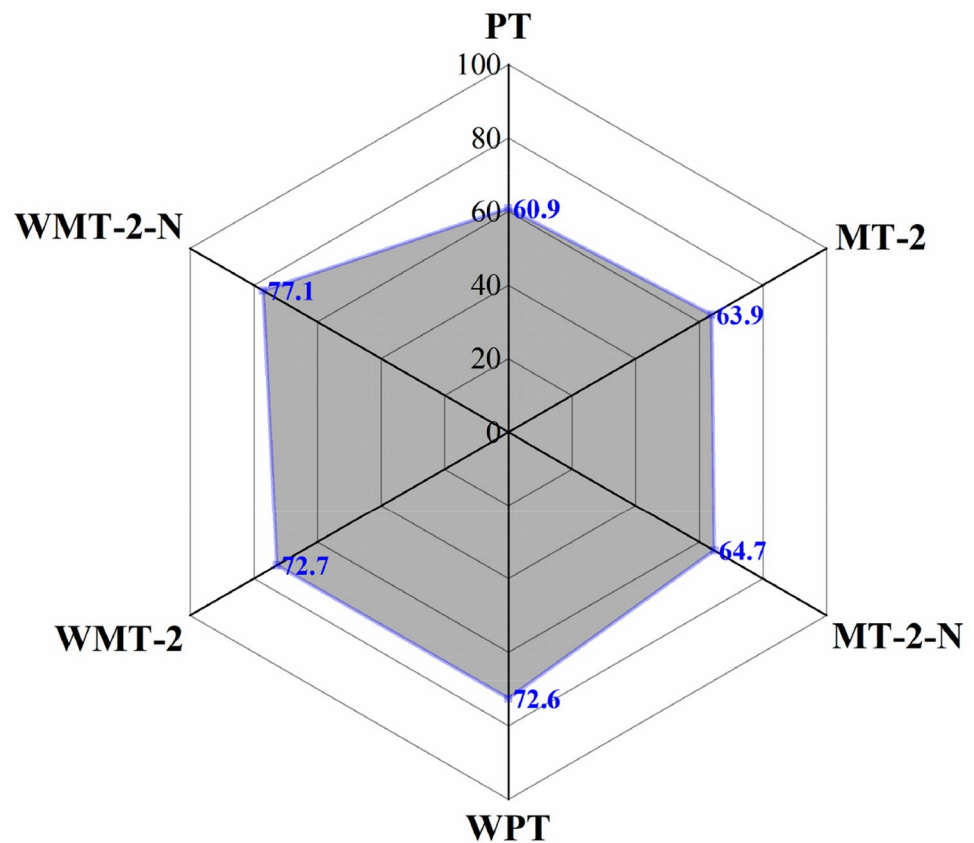
In this paper, dry cutting AISI1045 steel using cutting tools configured with shark-skin-inspired structures and WS₂/C coatings was investigated. The electrohydrodynamic atomization method to prepare WS₂/C coatings was determined by the analytical hierarchy process (AHP). The dry cutting performance of cutting tools with different treatments was studied. The assessment of sustainable manufacturing capability was carried out. Some conclusions were drawn as follows:

- (1) AHP was used to choose an appropriate method of depositing WS₂/C coating for dry cutting tools, taking into account the criteria of coating property, deposition process, resource and equipment. WS₂/C coatings deposited by the electrohydrodynamic atomization method were more suitable in comparison with magnetron deposition and cathode-arc deposition methods.
- (2) Among all six cutting tools (PT, MT-2, MT-2-N, WPT, WMT-2 and WMT-2-N), dry cutting AISI1045 steel using WMT-2-N tools have shown excellent cutting performances in terms of (1) reduced cutting forces

Table 4 PSI for all cutting tools under the dry cutting condition

Tools	Energy consumption	Manufacturing cost	Machined surface roughness	Workpiece cleaning	Scrap disposal	Environmental effect	Operator health and safety	PSI
PT	7.9	1.8	2.4	10	9	6.5	5	60.9
MT-2	7.4	2.1	3.2	10	9	7	6	63.9
MT-2-N	7.4	2.2	3.7	10	9	7	6	64.7
WPT	7.2	3.5	5.1	10	9	8	8	72.6
WMT-2	7	3.2	5.7	10	9	8	8	72.7
WMT-2-N	7	4	6	10	9	9	9	77.1

Fig. 20 Total PSI of all cutting tools for sustainability assessment



and cutting temperatures, (2) increased specific cutting energy and minimum machined surface roughness, (3) slight tool wear (rake and flank wear) and longer tool life.

- (3) The sustainability assessment by PSI calculation showed that dry cutting experiments using WMT-2-N tools had the highest total PSI of 78.6%, and can be one of the best practical choices for achieving sustainable manufacturing. These results can be considered as one reference for sustainability evaluation when dry-cutting various workpiece material using cutting tools configured with textured surfaces and lubricating coatings. It should be noted that more influencing factors for sustainability assessment should be added or modified in order to suit some specific machining conditions.

Supplementary Information The online version contains supplementary material available at <https://doi.org/10.1007/s40684-021-00330-x>.

Acknowledgements This work is supported by the Natural Science Foundation of Shandong Province (ZR2018ZB0522), National Natural Science Foundation of China (51675311) and the China Scholarship Council.

Declarations

Conflict of interest The authors declare that they have no known competing financial interests or personal relationships that could have appeared to influence the work reported in this paper.

References

- Chetan, Ghosh, S., & Venkateswara Rao, P. (2015). Application of sustainable techniques in metal cutting for enhanced machinability: a review. *Journal of Cleaner Production*, 100, 17–34. <https://doi.org/10.1016/j.jclepro.2015.03.039>
- Jayal, A. D., Badurdeen, F., Dillon, O. W., & Jawahir, I. S. (2010). Sustainable manufacturing: modeling and optimization challenges at the product, process and system levels. *CIRP Journal of Manufacturing Science and Technology*, 2, 144–152. <https://doi.org/10.1016/j.cirpj.2010.03.006>
- Moldavska, A., & Welo, T. (2017). The concept of sustainable manufacturing and its definitions: a content-analysis based literature review. *Journal of Cleaner Production*. <https://doi.org/10.1016/j.jclepro.2017.08.006>
- Motyka, M., Ziaja, W., Sieniawski, J. (2017). Titanium alloys novel aspects of their manufacturing and processing. *IntechOpen*. 2019. <https://doi.org/10.5772/intechopen.82344>
- Pusavec, F., Krajnik, P., & Kopac, J. (2010). Transitioning to sustainable production—Part I: application on machining

- technologies. *Journal of Cleaner Production*, 18, 174–184. <https://doi.org/10.1016/j.jclepro.2009.08.010>
6. Klocke, F., & Eisenblätter, G. (1997). Dry cutting. *CIRP Annals*, 46, 519–526. [https://doi.org/10.1016/S0007-8506\(07\)60877-4](https://doi.org/10.1016/S0007-8506(07)60877-4)
 7. Marksberry, P. W. (2007). Micro-flood (MF) technology for sustainable manufacturing operations that are coolant less and occupationally friendly. *Journal of Cleaner Production*, 15, 958–971. <https://doi.org/10.1016/j.jclepro.2006.01.006>
 8. Calvert, G. M., Ward, E., Schnorr, T. M., & Fine, L. J. (1998). Cancer risks among workers exposed to metalworking fluids: a systematic review. *American Journal of Industrial Medicine*, 33, 282–292. [https://doi.org/10.1002/\(sici\)1097-0274\(199803\)33:3%3c282::aid-ajim10%3e3.0.co;2-w](https://doi.org/10.1002/(sici)1097-0274(199803)33:3%3c282::aid-ajim10%3e3.0.co;2-w)
 9. Abdelrazek, A. H., Choudhury, I. A., Nukman, Y., & Kazi, S. N. (2020). Metal cutting lubricants and cutting tools: a review on the performance improvement and sustainability assessment. *International Journal of Advanced Manufacturing Technology*, 106, 4221–4245. <https://doi.org/10.1007/s00170-019-04890-w>
 10. Narasimhulu, A., Ghosh, S., & Rao, P. V. (2015). Study of tool wear mechanisms and mathematical modeling of flank wear during machining of Ti alloy (Ti6Al4V). *Journal of The Institution of Engineers (India) Series C*, 96, 279. <https://doi.org/10.1007/s40032-014-0162-9>
 11. Sharma, V. S., Dogra, M., & Suri, N. M. (2009). Cooling techniques for improved productivity in turning. *International Journal of Machine Tools and Manufacture*, 49, 435–453. <https://doi.org/10.1016/j.ijmactools.2008.12.010>
 12. Li, X., Deng, J., Ge, D., & Yue, H. (2020). Rapid crystallization of electrohydrodynamically atomized ZrO₂ thin films by laser annealing. *Applied Surface Science*, 510, 145510. <https://doi.org/10.1016/j.apsusc.2020.145510>
 13. Sadeghzade, S., Emadi, R., Tavangarian, F., & Doostmohammadi, A. (2020). The influence of polycaprolacton fumarate coating on mechanical properties and in vitro behavior of porous diopside-hardystonite nano-composite scaffold. *Journal of the Mechanical Behavior of Biomedical Materials*, 101, 103445. <https://doi.org/10.1016/j.jmbbm.2019.103445>
 14. Karthick, S., Shalini, S., Mani Prabu, S. S., Suhel, K., Vandan, A., Puneet, C., Manoj Kumar, S., Venkatesh, R., & Palani, I. A. (2020). Influence of quaternary alloying addition on transformation temperatures and shape memory properties of Cu–Al–Mn shape memory alloy coated optical fiber. *Measurement*, 153, 107379. <https://doi.org/10.1016/j.measurement.2019.107379>
 15. Domínguez-Meister, S., Conte, M., Igartua, A., Rojas, T. C., & Sanchez-Lopez, J. C. (2015). Self-lubricity of WSex nanocomposite coatings. *ACS Applied Materials and Interfaces*, 7, 7979–7986. <https://doi.org/10.1021/am508939s>
 16. Lian, Y., Chen, H., Mu, C., Deng, J., & Lei, S. (2018). Experimental investigation and mechanism analysis of tungsten disulfide soft coated micro-nano textured self-lubricating dry cutting tools. *International Journal of Precision Engineering and Manufacturing-Green Technology*, 5, 219–230. <https://doi.org/10.1007/s40684-018-0022-9>
 17. Xing, Y., Wu, Z., Yang, J., Wang, X., & Liu, L. (2020). LIPSS combined with ALD MoS₂ nano-coatings for enhancing surface friction and hydrophobic performances. *Surface and Coatings Technology*, 385, 125396. <https://doi.org/10.1016/j.surfcoat.2020.125396>
 18. Tyagi, R., Das, A. K., & Mandal, A. (2018). Electrical discharge coating using WS₂ and Cu powder mixture for solid lubrication and enhanced tribological performance. *Tribology International*, 120, 80–92. <https://doi.org/10.1016/j.triboint.2017.12.023>
 19. Ding, X., Zeng, X. T., He, X. Y., & Chen, Z. (2010). Tribological properties of Cr- and Ti-doped MoS₂ composite coatings under different humidity atmosphere. *Surface and Coatings Technology*, 205, 224–231. <https://doi.org/10.1016/j.surfcoat.2010.06.041>
 20. Banerji, A., Bhowmick, S., & Alpas, A. T. (2016). Role of temperature on tribological behaviour of Ti containing MoS₂ coating against aluminum alloys. *Surface and Coatings Technology*. <https://doi.org/10.1016/j.surfcoat.2016.09.044>
 21. Zhang, X., Qiao, L., Chai, L., Xu, J., Shi, L., & Wang, P. (2016). Structural, mechanical and tribological properties of Mo–S–N solid lubricant films. *Surface and Coatings Technology*, 296, 185–191. <https://doi.org/10.1016/j.surfcoat.2016.04.040>
 22. Xu, J., Chai, L., Qiao, L., He, T., & Wang, P. (2016). Influence of C dopant on the structure, mechanical and tribological properties of r.f.-sputtered MoS₂/a-C composite films. *Applied Surface Science*, 364, 249–256. <https://doi.org/10.1016/j.apsusc.2015.12.152>
 23. Zeleny, J. (1914). The electrical discharge from liquid points, and a hydrostatic method of measuring the electric intensity at their surfaces. *Physical Review*, 3, 69–91. <https://doi.org/10.1103/PhysRev.3.69>
 24. Li, X., Deng, J., Yue, H., Ge, D., & Zou, X. (2019). Wear performance of electrohydrodynamically atomized WS₂ coatings deposited on biomimetic shark-skin textured surfaces. *Tribology International*, 134, 240–251. <https://doi.org/10.1016/j.triboint.2019.02.015>
 25. Li, X., Deng, J., Liu, L., Zhang, L., Sun, J., Ge, D., Liu, Y., & Duan, R. (2018). Tribological properties of WS₂ coatings deposited on textured surfaces by electrohydrodynamic atomization. *Surface and Coatings Technology*, 352, 128–143. <https://doi.org/10.1016/j.surfcoat.2018.08.011>
 26. Zhang, J., Lee, Y. J., & Wang, H. (2020). Surface texture transformation in micro-cutting of AA6061-T6 with the rebinder effect. *International Journal of Precision Engineering and Manufacturing-Green Technology*. <https://doi.org/10.1007/s40684-020-00260-0>
 27. Wei, Y., Kim, M.-R., Lee, D.-W., Park, C., & Park, S. S. (2017). Effects of micro textured sapphire tool regarding cutting forces in turning operations. *International Journal of Precision Engineering and Manufacturing-Green Technology*, 4, 141–147. <https://doi.org/10.1007/s40684-017-0017-y>
 28. Kawasegi, N., Sugimori, H., Morimoto, H., Morita, N., & Hori, I. (2009). Development of cutting tools with microscale and nanoscale textures to improve frictional behavior. *Precision Engineering*, 33, 248–254. <https://doi.org/10.1016/j.precisioneng.2008.07.005>
 29. Jianxin, D., Ze, W., Yunsong, L., Ting, Q., & Jie, C. (2012). Performance of carbide tools with textured rake-face filled with solid lubricants in dry cutting processes. *International Journal of Refractory Metals and Hard Materials*, 30, 164–172. <https://doi.org/10.1016/j.ijrmhm.2011.08.002>
 30. Sugihara, T., & Enomoto, T. (2009). Development of a cutting tool with a textured surface for dry cutting of aluminum alloys. *International Journal of Automation Technology*, 3, 199–203. <https://doi.org/10.20965/ijat.2009.p0199>
 31. Wang, Y., Li, N., Ma, Y., Tong, J., Pflieger, W., & Sun, J. (2020). Field experiments evaluating a biomimetic shark-inspired (BioS) subsoiler for tillage resistance reduction. *Soil and Tillage Research*, 196, 104432. <https://doi.org/10.1016/j.still.2019.104432>
 32. Fatima, A., & Mativenga, P. (2015). On the comparative cutting performance of nature-inspired structured cutting tool in dry cutting of AISI/SAE 4140. *Proceedings of the Institution of Mechanical Engineers Part B Journal of Engineering Manufacture*. <https://doi.org/10.1177/0954405415617930>
 33. Wan, C., & Gorb, S. (2019). Friction Reduction Mechanism of the Cuticle Surface in the Sandhopper *Talitrus Saltator* (Amphipoda, Talitridae): Acta Biomaterialia. <https://doi.org/10.1016/j.actbio.2019.10.031>
 34. Lu, Y., Hua, M., & Liu, Z. (2014). The biomimetic shark skin optimization design method for improving lubrication effect of

- engineering surface. *Journal of Tribology*, 136, 317031–3170313. <https://doi.org/10.1115/1.4026972>
35. Li, X., Deng, J., Lu, Y., Zhang, L., Sun, J., & Wu, F. (2019). Tribological behavior of ZrO₂/WS₂ coating surfaces with biomimetic shark-skin structure. *Ceramics International*, 45, 21759–21767. <https://doi.org/10.1016/j.ceramint.2019.07.177>
 36. Zhang, Y., Wang, R., Huang, P., Wang, X., & Wang, S. (2020). Risk evaluation of large-scale seawater desalination projects based on an integrated fuzzy comprehensive evaluation and analytic hierarchy process method. *Desalination*, 478, 114286. <https://doi.org/10.1016/j.desal.2019.114286>
 37. Zhang, K., Deng, J., Meng, R., Gao, P., & Yue, H. (2015). Effect of nano-scale textures on cutting performance of WC/Co-based Ti55Al45N coated tools in dry cutting. *International Journal of Refractory Metals and Hard Materials*. <https://doi.org/10.1016/j.ijrmhm.2015.02.011>
 38. Scharf, T. W., Prasad, S. V., Dugger, M. T., Kotula, P. G., Goetze, R. S., & Grubbs, R. K. (2006). Growth, structure, and tribological behavior of atomic layer-deposited tungsten disulphide solid lubricant coatings with applications to MEMS. *Acta Materialia*, 54, 4731–4743. <https://doi.org/10.1016/j.actamat.2006.06.009>
 39. Von Lim, Y., Wang, Y., Guo, L., Kong, D., Ang, L. K., Wong, J., & Yang, H. Y. (2017). Cubic-shaped WS₂ nanopetals on Prussian blue derived nitrogen-doped carbon nanoporous framework for high performance sodium-ion batteries. *Journal of Materials Chemistry A*. <https://doi.org/10.1039/C7TA01821E>
 40. Braham-Bouchnak, T., Germain, G., Morel, A., & Furet, B. (2015). Influence of high-pressure coolant assistance on the machinability of the titanium alloy Ti555–3. *Machining Science and Technology*, 19, 134–151. <https://doi.org/10.1080/10910344.2014.991029>
 41. Song, W., Wang, Z., Wang, S., Zhou, K., & Guo, Z. (2017). Experimental study on the cutting temperature of textured carbide tool embedded with graphite. *International Journal of Advanced Manufacturing Technology*, 93, 3419–3427. <https://doi.org/10.1007/s00170-017-0683-5>
 42. Shaw, M. C. (1984). *Metal Cutting Principles*. New York: Oxford University Press.
 43. Groover, M. P. (2010). *Fundamentals of modern manufacturing: materials, processes, and systems* (4th ed.). New York: John Wiley & Sons.
 44. Padhan, S., Das, A., Santoshwar, A., Dharmendrabhai, T. R., & Das, S. R. (2020). Sustainability assessment and machinability investigation of austenitic stainless steel in finish turning with advanced ultra-hard SiAlON ceramic tool under different cutting environments. *Silicon*. <https://doi.org/10.1007/s12633-020-00409-1>
 45. Kadam, G., & Pawade, R. (2017). Surface integrity and sustainability assessment in high-speed machining of Inconel 718—an eco-friendly green approach. *Journal of Cleaner Production*. <https://doi.org/10.1016/j.jclepro.2017.01.104>
 46. Zhao, D., Tian, Q., Wang, M., & Jin, Y. (2014). Study on the hydrophobic property of shark-skin-inspired micro-riblets. *Journal of Bionic Engineering*, 11, 296–302. [https://doi.org/10.1016/S1672-6529\(14\)60046-9](https://doi.org/10.1016/S1672-6529(14)60046-9)
 47. Hamdi, A., Bouchelaghem, H., Yaltese, M., Mohamed, E., & Fnides, B. (2014). Machinability investigation in hard turning of AISI D3 cold work steel with ceramic tool using response surface methodology. *International Journal of Advanced Manufacturing Technology*, 73, 1775–1788. <https://doi.org/10.1007/s00170-014-5950-0>
 48. Jamil, M., Khan, A. M., He, N., Li, L., Iqbal, A., & Mia, M. (2019). Evaluation of machinability and economic performance in cryogenic-assisted hard turning of α - β titanium: a step towards sustainable manufacturing. *Machining Science and Technology*, 23, 1022–1046. <https://doi.org/10.1080/10910344.2019.1652312>

Publisher's Note Springer Nature remains neutral with regard to jurisdictional claims in published maps and institutional affiliations.



Xuemu Li Ph.D. candidate in the key laboratory of high efficiency and clean mechanical manufacture of MOE, school of mechanical engineering, Shandong university. His primary research interest is micro-nano manufacturing technology.



Jianxin Deng He received the Ph.D. degree in mechanical engineering from school of mechanical engineering, Shandong University in 1995. He is currently a professor in the school of mechanical engineering at Shandong University. He is a senior member of the Chinese Mechanical Engineering Society. His research interests include high speed machining, ceramic cutting tools, self-lubrication tools and ceramic nozzles in abrasive machining.



Yang Lu Ph.D. candidate in the key laboratory of high efficiency and clean mechanical manufacture of MOE, school of mechanical engineering, Shandong university. His primary research interest is dry machining of textured tools.



Ran Duan He received the Ph.D. degree in mechanical engineering from school of mechanical engineering, Shandong University in 2020. He is currently a lecturer in the school of mechanical and electronic engineering, Shandong Jianzhu University. His research interest is derivative cutting of textured tools.



Dongliang Ge Ph.D. candidate in the key laboratory of high efficiency and clean mechanical manufacture of MOE, school of mechanical engineering, Shandong university. His research interest is dry machining of textured tools.